Clockwork Orangutan: microRNAs, thermoregulatory tradeoffs, and the evolution of brain size

Bastian Fromm, PhD**
UiT - The Arctic University of Norway,
The Arctic University Museum of Norway
9006 Tromsø, NO

Thomas Sorger, PhD*
Department of Biology
Roger Williams University
Bristol, RI 02809

*** Lead contact**
****Second corresponding author**

SUMMARY

Models of brain size evolution have not accounted for the thermoregulatory adaptations underlying the 4-fold increase in brain metabolic rate (*MR*) in hominid apes. Like earlier increases in whole-body *MR*, the advent of placentation and permanent homeothermy, the divergence of Catarrhini coincided with an adaptive increase in the number of microRNA families (*mirFam*). We demonstrate in mammals that the size of the brain, the primary consumer of glucose, and the liver, the primary organ of gluconeogenesis, vary inversely relative to a thermogenic Core (kidney + heart + liver + brain). The cellular *MR* (*cMR*) of the liver, scaled in proportion to *mirFam*, varied inversely with body size and the *cMR*s of kidney, heart and brain. With *mirFam* as a proxy for energy reliability, a logistic feedback model of relative brain size detected adaptation to a low-energy regime among the smallest primates and, among the largest primates, adaptation to the physiological limit on the rate of heat dissipation.

INTRODUCTION

The diversification of mammalian orders is characterized by two long-term trends: increasing size[1] and decreasing body temperature[2]. Resting metabolic rates (*rMR*s) do not exhibit a long-term trend but, in coordination with thermal conductance (C_{min}), have allowed most orders of mammals to occupy nearly every climatic zone regardless of size[3-4], albeit with a narrower range of tolerance to heat than to cold[5-7]. These observations support the evolutionary relevance of a physiological limit on the rate of heat dissipation[8-9], initially elaborated by Speakman and Król (2010)[10].

The recent publication of hundreds of primate genome sequences[11] has made possible ever more fine-grained analyses of the phylogenetic covariance of traits that may have fueled the 4-fold expansion of brain size[12] and acceleration of *MR*[13] in the hominid lineage: diets richer in calories and protein[14-15], more efficient food acquisition and assimilation[16], greater adipose tissue reserves[17-19], and gains in the reliability of gestation, lactation and infant care[20-21]. However, comparative phylogenetic models of brain size evolution[22-23] have yet to account for the underlying adaptations required to maintain thermal homeostasis.

Simulation of two million years of African and Eurasian climate and habitats supports the view that *H. sapiens* evolved from *H. heidelbergensis* in southern Africa during an unusually warm period that would have necessitated adaptation to hotter, drier conditions[24], consistent with the "Savanna hypothesis"[25-27]. Among hunter-gatherers and contemporary indigenous populations, both resting and

active *MR*s are elevated compared with those of non-human apes, necessitating a faster rate of heat dissipation[13] that has been enabled by uniquely human adaptations such as hairlessness, bipedalism, and a 10-fold increase in the density of eccrine sweat glands relative to the densities found in chimpanzees and macaques[28]. The latter adaptation may have enabled early humans to run down game in long distance pursuits[29], but may have also made them uniquely susceptible to dehydration[30], a marathon-enabling tradeoff.

Although similar in size to humans, orangutans have lower body temperatures[31] and lower active *MR*s[13] but their brains are ⅔ smaller and generate heat at a rate of only 4W, compared to 15W in humans[19]. This thermogenesis raises the temperature of the brain's venous outflow, 15% of total blood volume per minute[32-33], by 0.2° - 0.3°C[34], but does not trigger sweating and evaporative cooling to the same extent as physical activity. During exercise, human brain temperature increases in parallel with that of the body core, eventually leading to hyperthermia and fatigue[35]. Unlike arid-zone artiodactyls such as springbok, primates lack a carotid *rete*, a counter-current structure that can decrease brain temperature up to 0.5°C in animals at rest[36-37]. On the other hand, cooling of the brain, the only organ with its own exoskeleton, has been proposed as a benefit of the so-called "oxygen paradox" of neurovascular coupling *i.e.* the surplus blood flow in excess of oxygen demand, elicited by neuronal activation[38-40]. Another potential mechanism to address this thermoregulatory challenge, first proposed four decades ago, is a tradeoff in energy expenditure with another metabolically expensive tissue, such as kidney, heart, liver or intestine[41-42]. Despite numerous attempts, the effort to detect the tradeoff predicted by this "expensive tissue hypothesis" has been abandoned since the publication of a study encompassing 100 species, including 23 primates, that found no significant anticorrelations among the body mass-independent residuals of seven metabolically expensive organs[18].

Lande (1979)[43] attributed the evolutionary increase in primate brain size to a genetic uncoupling of its dependence on body size. We postulated that thermal homeostasis could be achieved by relaxing the constraint imposed by body size not only on the size of the brain, but also on the sizes of the three other major thermogenic organs (kidney, heart and liver). In this case, the relevant standard for the mass of these organs would be the mass of a composite 4-organ "Core", analogous to the thermoregulatory core predicted by the biophysical model of Porter and Kearney (2009)[44]. Relative to this core, we find that evolutionary increases in the proportion of the brain are offset by decreases in the proportion of the liver, with a corresponding anticorrelation between mass-independent residuals.

The evolutionary expansion of brain size in the human lineage, like the emergence of placentation and permanent homeothermy, depended on significant increases in *rMR*, together with compensatory mechanisms to maintain thermal homeostasis. With the emergence of 24-h control of body temperature, Boreoeutheria crossed a threshold of energy reliability relative to earlier-branching placentals and marsupials, among which many orders exhibit some degree of heterothermy[45-46], thereby setting the stage for their subsequent ecological diversification[47]. We have previously shown that the divergence of Boreoeutheria corresponded to adaptive increases in T_b and the number of microRNA families (*mirFam*), independent of body size, and that a model of stabilizing selection best accounted for the strong association between *mirFam* and cellular *MR* ($rMR/M^{0.75}$)[9]. The divergence of Catarrhini was also accompanied by a 15% increase in the average number of conserved microRNA families (*mirFam*), similar to these earlier expansions[48]. Thus, each increase in the range of *mirFam* has defined a new range of variation of *rMR* and *Mbdy* and, consequently, the range of brain size variation. If *mirFam* can serve as an index of energy reliability, then within each clade, heterotherms would be predicted to occupy the low end of the range of *mirFam* variation, which appears to be the case[9, 49].

In order to compare the evolution of the rates of thermogenesis among these four organs, we estimated their cellular *MR*s (*cMR*s) according to three criteria:

a) correlation with *mirFam*, corrected for organ size (physiological relevance)[9];
b) equivalence between the joint *cMR* of the four Core organs and the predicted rate of core thermogenesis, which scales as ~ $\sqrt{M}$[44] (thermodynamic relevance);
c) utility for the unsupervised classification of major primate clades (phylogenetic relevance).

We find that *mirFam*-based liver *cMR*s are strictly anticorrelated with body mass and the *cMR*s of kidney, heart and brain. Since the liver is the primary organ of gluconeogenesis during fasting or starvation, the tradeoffs between liver and brain in size and *cMR* are consistent with a positive feedback model of brain size evolution, governed by energy reliability[22, 23].

The effectiveness of this reparametrization of *cMR*s raises fundamental questions with regard to the relevant scaling of mass-corrected metabolic rate, with implications for covariance models of trait evolution[50-53]. The conventional inference of specific *MR* (*sMR*), based on the slope of log *rMR versus* log *Mbdy*, is theoretically questionable for several reasons:

a) the essential non-independence of *rMR* and *Mbdy*, a factor that is diminished when fitting the distribution of c*MR* (rMR/M^{exp}) to variables that vary only indirectly with body size;

b) the average ratio of *rMRbdy/Mbdy decreases* with size, consistent with surface area considerations, while the log ratio *increases* with size, leading to contrary rank orders when comparing clades with different size ranges, *e.g.* rodents *versus* primates;

c) while conventional s*MR*s depend on regression of log *rMR* on log *M* over several orders of magnitude, the standard $rMR/M^{0.75}$ ratio varies only twofold across mammalian orders and has adapted to ecological variables that scale arithmetically, notably temperature and aridity.

RESULTS

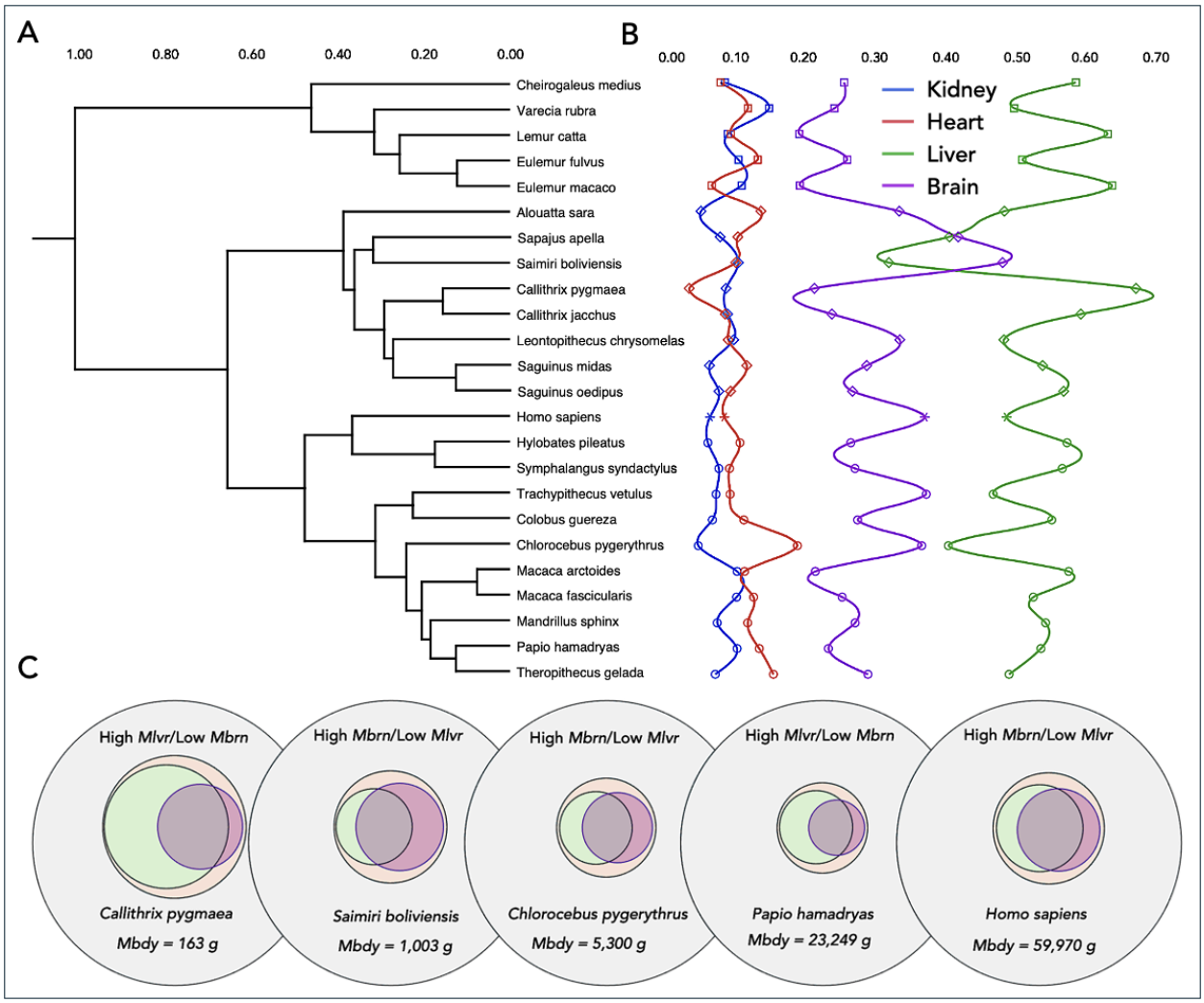

Figure 1. The proportion of brain mass in the thermogenic Core varies reciprocally with that of the liver.
A. Time tree of 24 primates. The scale bar represents the relative time of divergence.
B. Mass proportion of each organ relative to the total Core mass.
C. Summary comparing representative species with relatively low or high ratios of brain/liver mass. The radius of each circle represents a spherical volume proportional to organ or Core mass. The relative sizes of liver and brain are represented by green and purple circles, respectively. Silhouettes: *Callithrix jacchus*, *Saimiri* (generic), *Erythrocebus patas*, *Papio* (generic), *Homo sapiens idaltu* (© Phylopic 2024, compiled by T. Michael Keesey.

The proportion of brain mass in the Core varies reciprocally with that of liver

Of the six possible tradeoffs among four thermogenic organs, two occurred consistently in primate clades, that between brain and liver, and a dampened tradeoff between heart and kidney (Figure 1-B). Similar tradeoffs were observed among Glires, Laurasiatheria, Marsupialia, and an Afrotherian (Supplementary Figures S1 and S2). The two species exhibiting the highest brain/Core mass ratios were the largest terrestrial mammal (*Elephas maximus*) and the smallest weasel (*Mustela nivalis*).

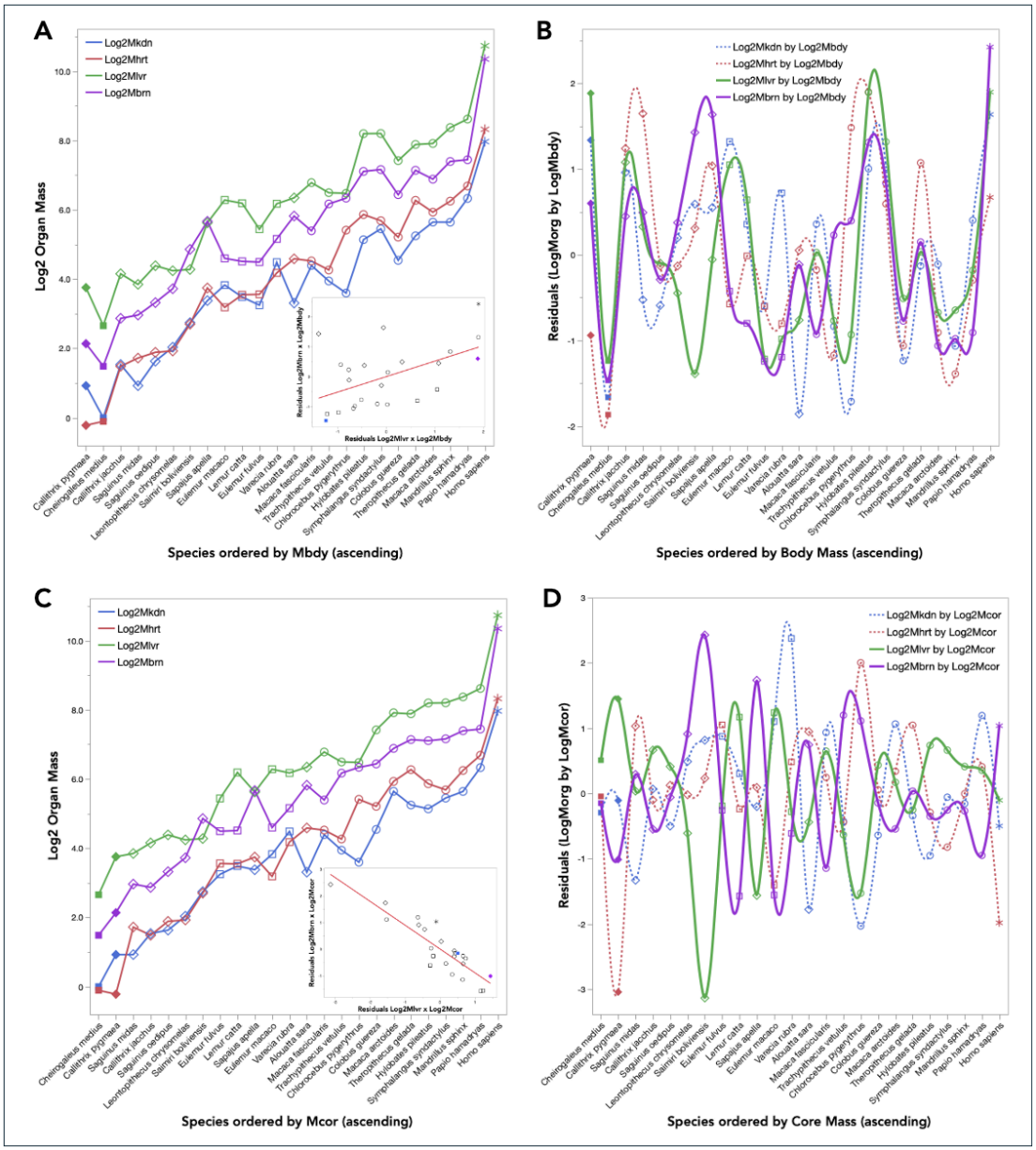

Figure 2. Variation of liver and brain mass relative to either the whole body or the four-organ Core.
A and C: Variation of organ size relative to body size and Core size in primates (N = 24).
Inset graphs: conventional residual plots for log *Mbrn versus* log *Mlvr* regressed against either log *Mbdy* (A) or log *Mcor* (C). R^2 = 0.23 (P = 9.63e-03) and 0.79 (P = 5.03e-09), respectively.
B and D: Mass-independent residual variation relative to body size and Core size in primates.

A tradeoff between liver and brain mass is also readily demonstrable in log-transformed data, provided that they are ranked according to Core size (Figure 2-C), rather than body size (Figure 2-A). Residuals of mass-independent regressions exhibited a periodic pattern of variation for each organ, corresponding to the relative proportion of body mass (Figure 2-B) or Core mass (Figure 2-D). Thus, standardization of log *Mbrn* with respect to log *Mbdy* has precluded detection of these tradeoffs[18].

Physiologically-based cMRs do not correspond to log-based sMRs

Assuming power law models, we distinguish between:

specific *MR* (*sMR*): $sMR = m \times M^b$,

where *b* is the slope of log *rMR*/log *M*, and

cellular *MR* (*cMR*): $cMR = n \times M^c$,

where *c* is the allometric exponent obtained by maximum likelihood fitting of rMR/M^c to the distribution of a physiologically-relevant trait, such as *mirFam*[9]. In the present report, "*rMR*" includes metabolic rates measured under basal conditions *i.e. bMR*s. Unlike log-based *sMRsmirFam*-based cellular *MR*s (*cMR*s) are sensitive to body temperature and robust to variation in the range of mass[9].

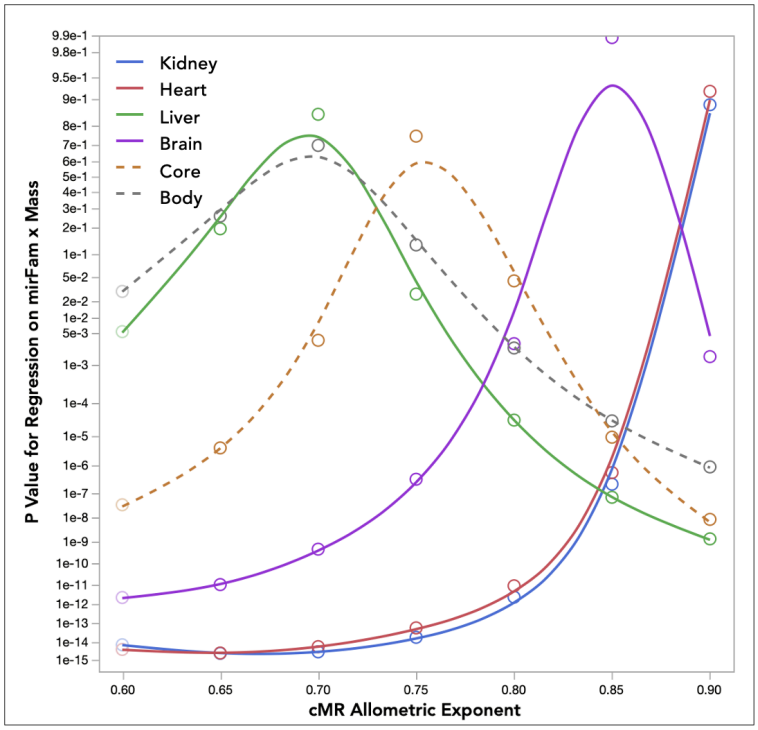

Figure 3. Dependence of *cMR* on *mirFam* and √*Morg* ($Morg^{0.5}$) (51 Euarchontoglires).
P values for regressions of organ *cMR* on √*Morg* and *mirFam* (binned – see Methods).
Regression on √*Morg* yielded *P* values several orders of magnitude lower than regression on log *Morg*.
Note that the the range $M^{0.70}$ - $M^{0.80}$ defines the limits of a zone of minimal correlation for the Core *cMR,* centered at $M^{0.75}$, and corresponding to the optimal scaling in a model of stabilizing selection[9].

Estimation of thermogenic organ cMRs

The context for our method is that the variation of mammalian *cMR* with respect to *mirFam* best fit a model of stabilizing selection when whole-body *cMR* was scaled to $M^{0.75}$ (hence "*cMR.75bdy*")[9]. In order to estimate a *mirFam*-based *cMR* for each thermogenic organ, we compared *cMR* dependence on both *mirFam* and organ mass in the range *cMR.60* - *cMR.90*, revealing opposite directions of correlation: increasing *P* values for kidney, heart and brain and decreasing *P* values for liver and whole body (Figure 3). Regression on *mirFam* or binned *mirFam* alone, without correction for organ mass, yielded essentially the same patterns, the only difference being a shift in the peak of the distribution of *P* values for *cMRbdy* from $M^{0.70}$ to $M^{0.75}$ (Supplementary Figure S3).

Assuming an operating range of $M^{0.70}$ - $M^{0.80}$, we estimated each organ *cMR* based on the lowest *P* value in this range, hence:

*cMR.**70**kdn*, *cMR.**70**hrt*, *cMR.**70**brn* and *cMR.**80**lvr*.

For each organ, the log-based *sMR* corresponded to the crossover point for the inversion of the *cMR* slopes with respect to organ size *i.e.* the zone of greatest mass-independent variation (Figure 4). Again, there was an obvious distinction between the allometric exponent for slope inversions for kidney, heart and brain (~ *cMR.85*) (Figure 4-A) and the exponent corresponding to the slope inversions for liver and whole body (~ *MR.70*) (Figure 4-B). Only the Core *cMR* exhibited an intermediate slope inversion (~ $M^{0.75}$) and log-based *sMR* ($M^{0.756}$) corresponding to Kleiber's allometric exponent for mammalian *sMR* (Figure 4-B)[54]. $M^{0.75}$ was previously shown to be the optimal scaling for a model of stabilizing selection of mammalian *cMR* with respect to *mirFam*[9], suggesting that the highly conserved relationship between the whole body rate of energy expenditure and body size represents a zone of minimal body size constraint on Core *cMR*.

Plotting the *cMR*s as a function of body size revealed fundamental differences between *cMR.80lvr*, on the one hand, and the *cMR.70*s of the three other organs, on the other: while the latter increased directly with size, *cMR.80lvr* was strictly anticorrelated with body mass (Figure 5-A). Furthermore, the slopes for the regressions of kidney, heart and brain *cMR.70* were significantly higher in primates than in Glires, while the slope of *cMR.80lvr* was essentially unchanged across both clades (Figure 5-A). The same ranking of slopes (heart > kidney > brain) and anticorrelation with liver *cMR.80* was obtained when organ *cMR*s were regressed on the thermal conductance (C_{min}) of 20 Boreoeutheria (Figure 5-B), pointing to a common origin for these physiological and thermoregulatory relationships.

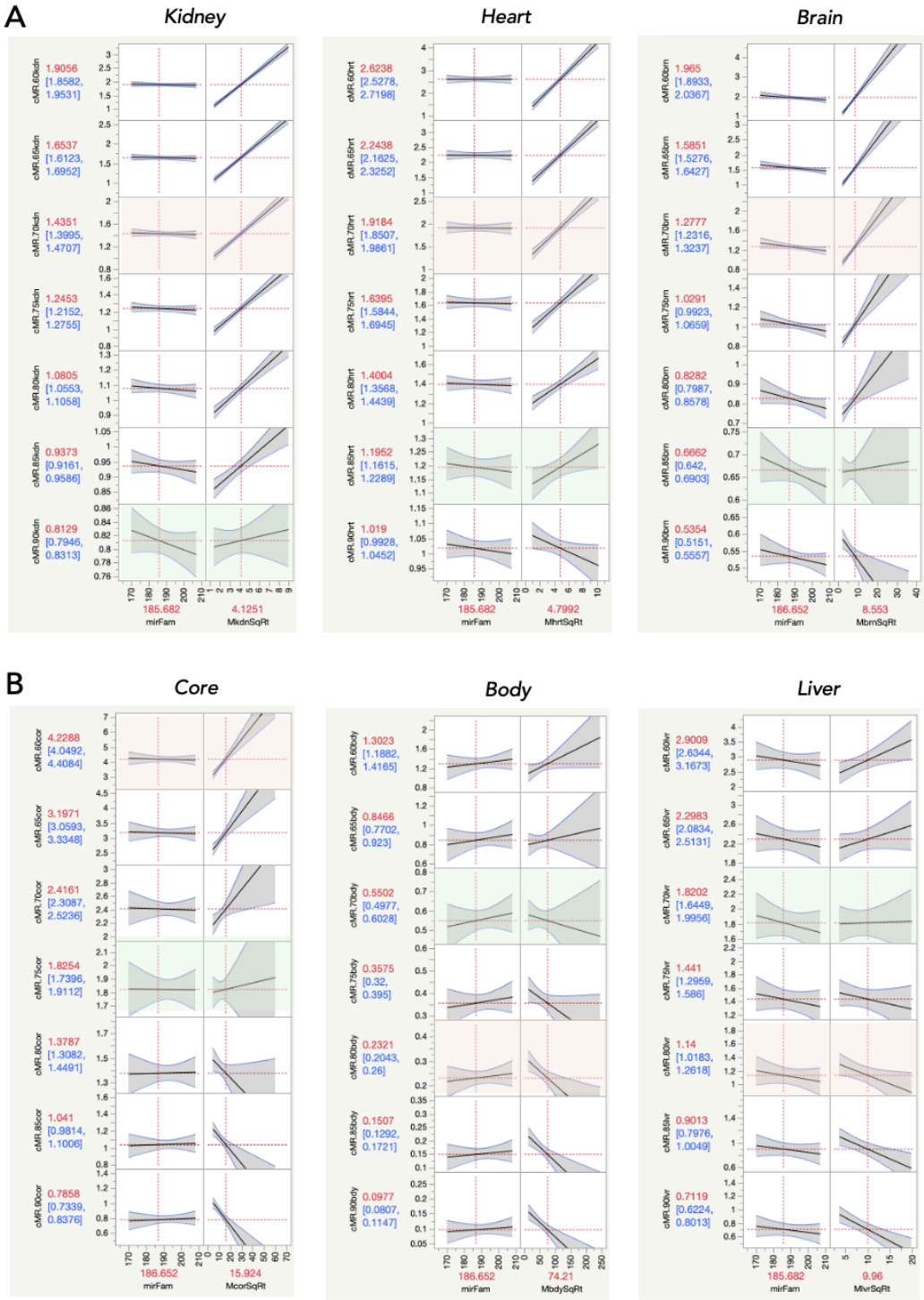

Figure 4. *cMR* slopes with respect to *mirFam* and $\sqrt{M}$, as a function of allometric exponent (22 primates). Estimated *cMR* slopes are shaded pink, log-based *sMR* slopes are shaded green. Grey bands represent CI. Note that log-based *sMR*s correspond to crossover points for the inversions of *cMR* slope with respect to $\sqrt{M}$.
A. Kidney, heart and brain *cMR*s exhibit similar patterns of slope inversion with respect to $\sqrt{M}$.
B. Liver and body *cMR*s exhibit similar slope inversions with respect to $\sqrt{M}$.
Only the Core *cMR* slopes invert at $M^{0.75}$. Values in red represent means ± CI (blue).

C_{min} is an extensive property that depends primarily on total body surface area and, secondarily, on the properties of the insulating layer[55]. When Boreoeutheria were ranked by the whole-body rate of heat generation (*cMR.75bdy*), *mirFam* tracked the whole-body rate of heat dissipation ($\log_2 C_{min}$) (Supplementary Figure S4-A), while ranking Boreoeutheria by C_{min} revealed tradeoffs between *cMR.80lvr* and *cMR.70brn* (Supplementary Figure S4-B). These associations reinforce the notion that the tradeoffs and variation in *mirFam* evolved in relation to thermoregulatory function.

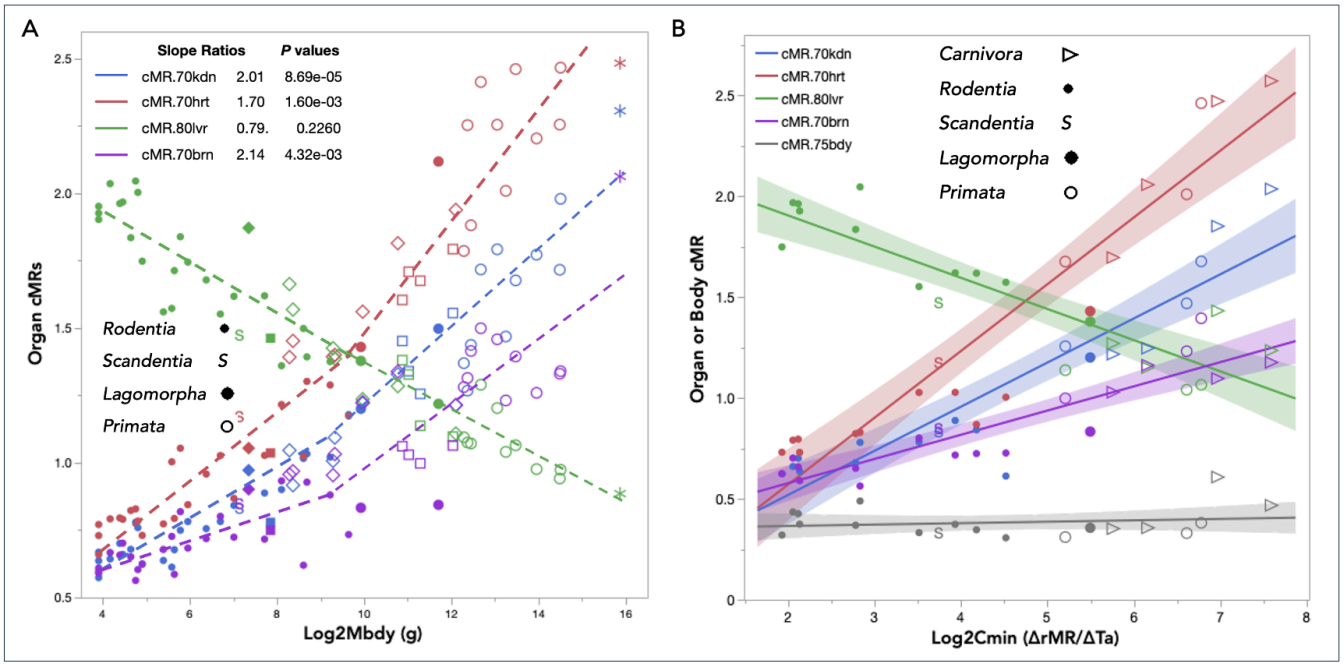

Figure 5. Core organ *cMR*s as a function of size or thermal conductance (*Cmin*).
A. Eaurchontoglires (N = 51). Slope ratios between primates and Glires were compared by ANCOVA.
B. Boreoeutheria (*N* = 23). T_a = ambient temperature. Shaded bands: confidence intervals (CI).

Thermodynamic and phylogenetic relevance of Core organ cMRs

We used linear models of *mirFam*-based *cMR*s in order to test two predictions of the thermogenic core model of Porter and Kearney (2009)[45]. Given that among mammals < 75 kg, the residual rate of thermogenesis, *i.e.* other than that of the four Core organs, averaged only 4.5% that of the liver[53]:
i) the joint *cMR* of the four most highly thermogenic organs, although delocalized, should scale approximately as the *cMR* of the geometrically centered core of the biophysical model (~ $M^{0.50}$);
ii) the joint *sMR* of the thermogenic organs should scale approximately as $M^{0.75}$, since the individual organ *rMR*s were inferred from an additive model assuming a whole body *sMR* = 70 x $M^{0.75}$ [56].

Using partial least squares regression[57], we generated additive models in order to predict the optimal scaling of a joint Core *cMR* composed of either *mirFam*-based *cMR*s:

cMR.Xcor = (*rMRkdn* + *rMRhrt* + *rMRlvr* + *rMRbrn*) / (*Mkdn* + *Mhrt* + *Mlvr* + *Mbrn*)^X

= (a • *cMR.**70kdn***) + (b • *cMR.**70hrt***) + (c • *cMR.**80lvr***) + (d • *cMR.**70brn***)

or log-based *sMR*s:

sMR.Xcor = (*rMRkdn* + *rMRhrt* + *rMRlvr* + *rMRbrn*) / (*Mkdn* + *Mhrt* + *Mlvr* + *Mbrn*)^X

= (a' • *sMR.**90kdn***) + (b' • *sMR.**87hrt***) + (c' • *sMR.**67lvr***) + (d' • *sMR.**83brn***)

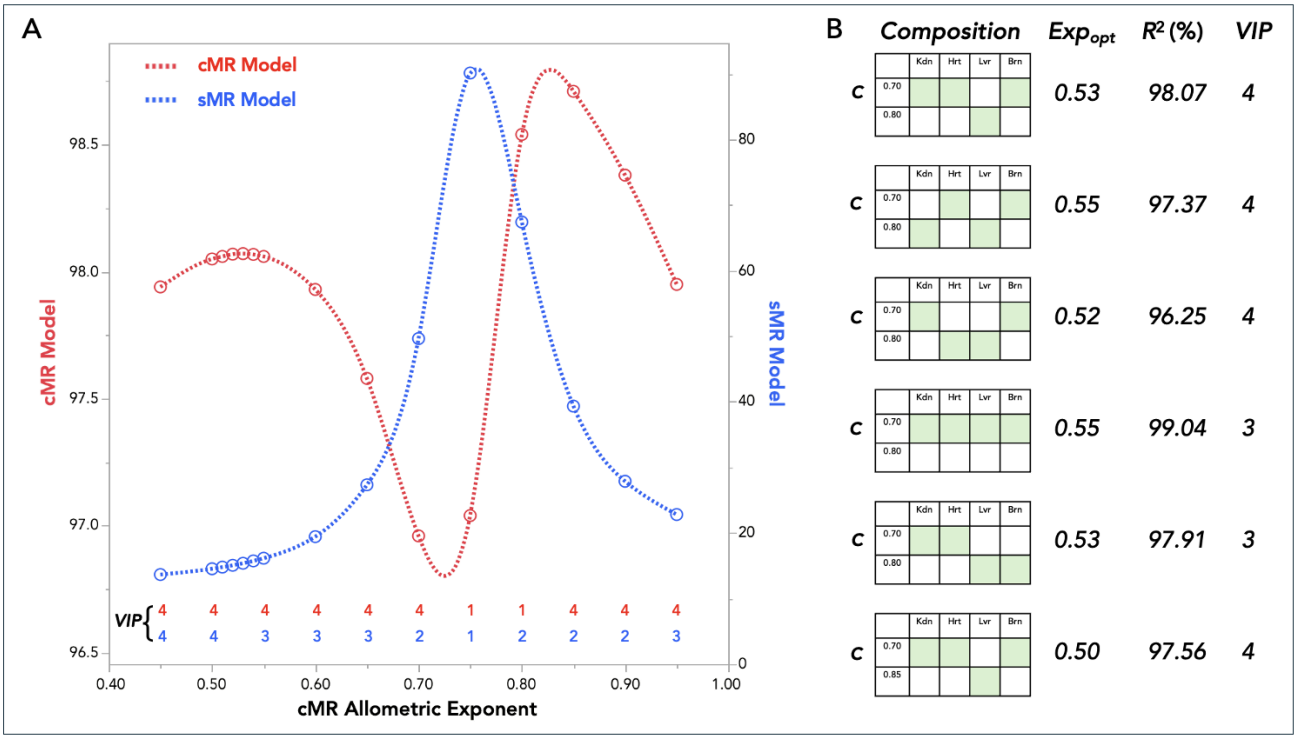

Figure 6. R^2 (% variation) for models of *cMRcor* predicted by linear combinations of the *mirFam*-based *cMR*s or log-based *sMR*s of the four thermogenic organs (note the difference between the scales) (*N* = 22).
A. Comparison between *mirFam*-based organ *cMR*s and log-based organ *sMR*s. Below the plot, the table of values for *VIP* (*variable importance of projection*) indicates the number of organs upon which each model is significantly dependent[58]. Curves were fit using the built-in spline method (JMP ©).
B. Comparison of the joint *cMR* of combinations of *cMR.70* and *cMR.80* among the four thermogenic organs. "*c*" is the organ *cMR* allometric exponent. "*Exp*$_{opt}$" is the optimally fitting allometric exponent of the model.

Among primates, the composite *cMR* model exhibited two peaks, one on either side of the inversion of Core *cMR* slopes with respect to √M: a broad peak centered at $M^{0.53}$, similar to that predicted by the biophysical model of core thermogenesis[45], and a second peak between $M^{0.80}$ - $M^{0.85}$ (Figure 6-A). The log-based joint *sMR* exhibited a single sharp peak at $M^{0.75}$, corresponding exactly to the model's assumed whole-body *sMR*[45]. Importantly, the *cMR* and *sMR* models exhibited critical differences in *VIP* statistics (*Variable Importance of Projection*[58]), a measure of the number of variables constraining each model (Figure 6-A). In the range *cMR.55cor* - *cMR.70cor*, only the *cMR* models depended on all

four organ *cMR*s (Figure 6-A). When scaled to $M^{0.75}$, both the *cMR* and *sMR* models of the Core were unconstrained by kidney, heart or brain, depending only on the *cMR* of the liver (Figure 6-A, bottom). We applied an additional test of the relevance of the estimated organ *cMR*s by comparing the joint *cMR*s obtained by permuting the combinations of the estimated organ *cMR*s, yielding four models with *VIP* = 4 (Figure 6-B). Two combinations were able to resolve Platyrrhini from Lemuriformes in an unsupervised classification of major primate clades[59]: either *cMR.80* or *cMR.85* for liver, together with *cMR.70* for heart, kidney and brain. When liver *cMR* was varied between *cMR.75* - *cMR.85*, the lowest value for the Bayes information criterion (BIC) corresponded to the originally estimated set of *mirFam*-based *cMR*s (Supplementary Figure S7):

cMR.53*cor =** 0.53 • ***cMR.70kdn **+** 0.69 • ***cMR.70hrt*** **+** 0.37 • ***cMR.80lvr*** **+** 0.09 • ***cMR.70brn***

In the context of the evolution of thermoregulation, the coefficient of each organ *cMR* in this model indicates its relative impact on the total rate of internal thermogenesis, from which one can infer the degree to which it has been constrained by natural selection *i.e.* the smaller its coefficient, the greater the degree of permitted evolutionary variation of the organ *cMR* since clade divergence.

The Core model represents a new approach to investigate the evolution of thermoregulation

The original biophysical model for thermoregulation assumed that metabolic heat emanates from the geometric center of an ellipsoid endotherm[44]. Depending on the wind condition or the presence of fur, the authors derived a single allometric exponent between 0.46 - 0.58 to scale the rate of core thermogenesis across the entire range of mammalian body size[44]. Since our Core model is delocalized among four thermogenic organs and makes no geometric assumptions, we expected lower allometric exponents ("c") and higher rates of thermogenesis (rMR/M^c) in smaller mammals with higher ratios of surface area/volume. Consistent with this expectation, the optimal allometric scaling of Core models developed in Carnivora, Primates and Glires were $M^{0.60}$, $M^{0.53}$ and $M^{0.40}$, respectively (Figure 7-A, B).

The values of the model parameters in Glires present a striking contrast to those in the carnivore and primate models: a reversal in sign of the coefficient for brain *cMR* in Glires, and a reversal of the relative magnitudes of the coefficients for liver and brain (Figure 7-A). Given that the median body size of Glires was only 1/80th that of primates (Supplementary Table S3), the observation that the Glires model penalizes the *cMR* of the brain suggests an adaptation to a disproportionate reduction of body size relative to brain size. Consequently, the median and average ratios of *Mbrn*/*Mbdy* have remained

higher in Glires than in primates or carnivora ($P < 0.001$, analysis of means), contrary to the rank order of log *Mbrn*/log *Mbdy* (Supplementary Table S3).

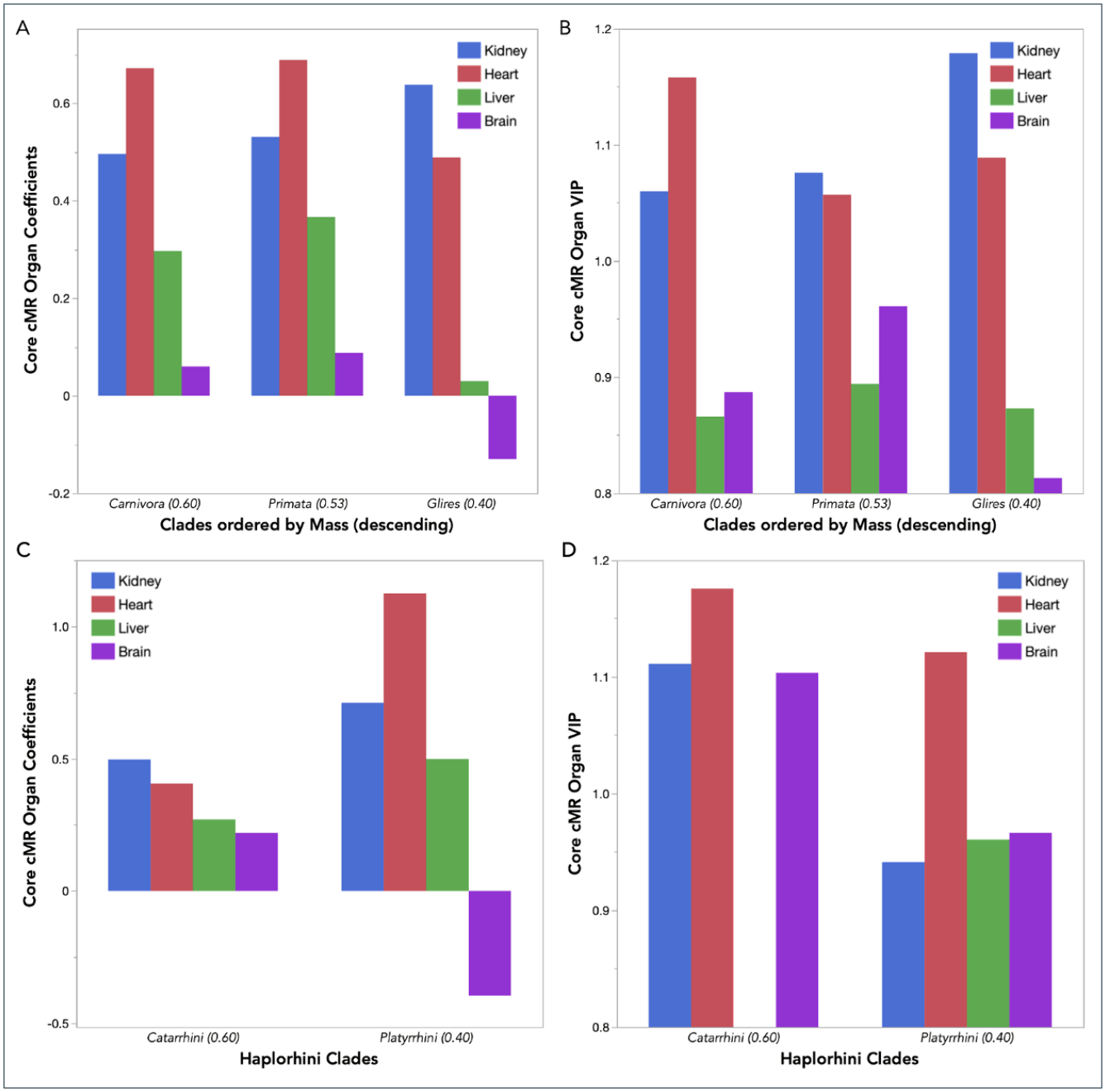

Figure 7. Organ *cMR* coefficients and *VIP* values for Core models in Boreoeutheria and Haplorhini.
Values in parentheses next to each clade indicate the optimal allometric exponent of the Core *cMR* model.
A. Organ coefficients for the optimal model for Carnivora ($N = 30$), Primata ($N = 22$) and Glires ($N = 26$).
B. Organ VIP values above threshold of significance (0.80) for each model.
C. Organ coefficients of the optimal models for Catarrhini ($N = 10$) and Platyrrhini ($N = 8$).
D. Organ VIP values above threshold of significance (0.80) for each model.
Note that in Catarrhini, the VIP for liver (0.4070) has dropped below the threshold of significance.

A converse pattern for the corresponding VIP values, reflecting the degree of constraint by each organ (Figure 7-B), was consistent with this interpretation. The same trends with respect to body size were recapitulated and magnified with the divergence of Platyrrhini from Catarrhini. The optimal Core *cMR* allometric exponent diverged from 0.53 for all primates, to 0.60 for the larger Catarrhini and 0.40 for the smaller Platyrrhini, consistent with surface area considerations (Figure 7-C). As in the case of the divergence of Glires from primates, the Platyrrhini model penalized the coefficient for brain *cMR* (Figure 7-C), while the average *Mbrn*/*Mbdy* ratio in Platyrrhini remained higher than in Catarrhini ($P < 0.001$, analysis of means), contrary to the order of log ratios (Supplementary Table S3). In Catarrhini, the VIP for liver dropped to 0.4070, below the 0.8 threshold for significance, indicating a negligible contribution to Core *cMR* model (Figure 7-D).

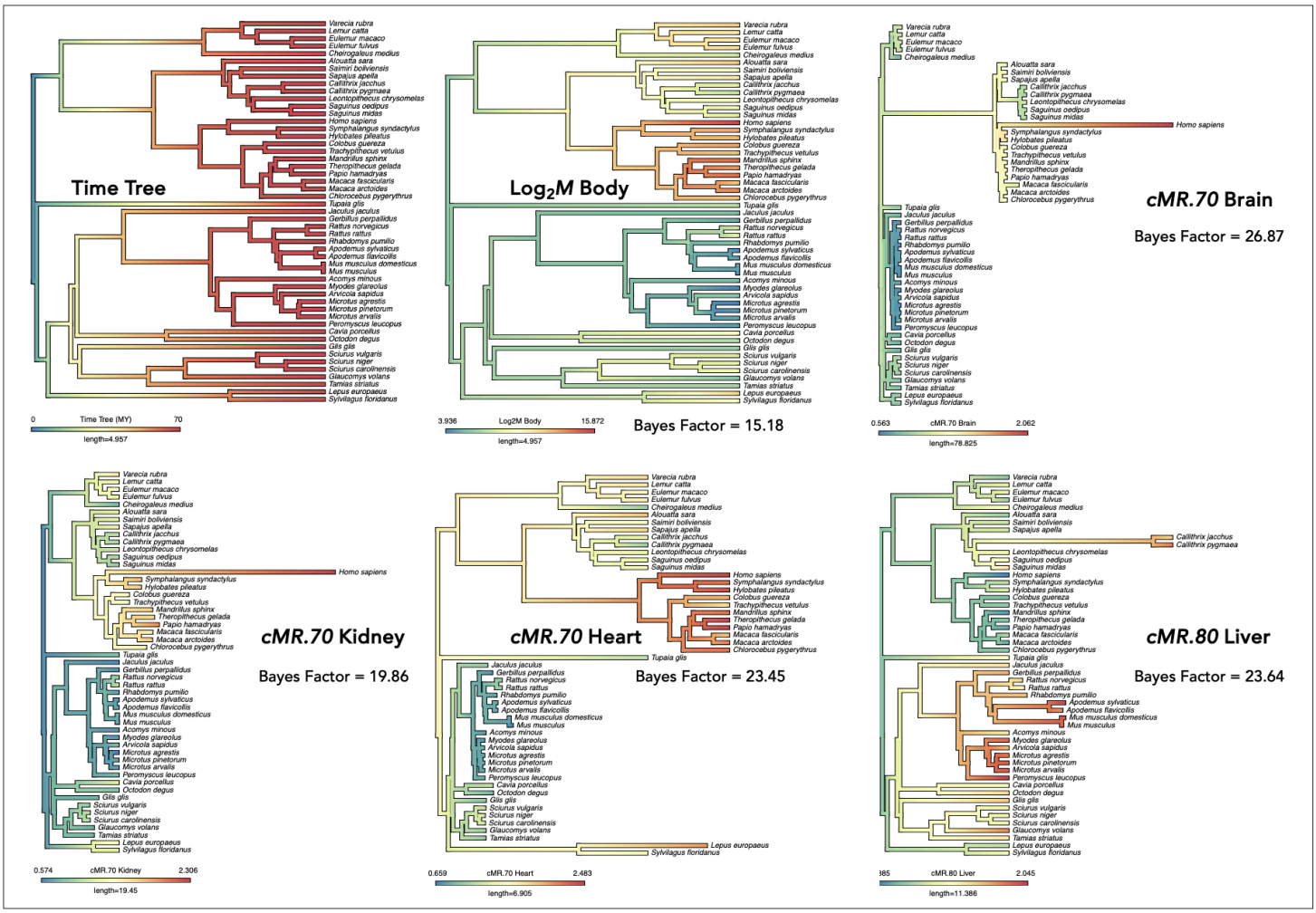

Figure 8. Variable rate phenograms of *Log Mbdy*, *cMR.80lvr*, and *cMR.70* of kidney, heart and brain.
The color values for the reference Time Tree depict the extent of underlying genomic evolution[61].
Bayes factors were computed from the difference in log likelihood (*Lh*) of the most likely trees and the trees with the smallest non-zero sum of changes to branch length, *i.e.* those trees most similar to the reference time tree[9].

Phylogenetic tradeoffs of mirFam-*based cMRs validate the Core model of thermoregulation*

The preceding evidence suggested that Boreoeutheria have been able to maintain thermal homeostasis while diversifying in body mass by fine-tuning the relative sizes and rates of thermogenesis of the four Core organs, particularly in the case of liver. We applied Bayesian inference in order to investigate the historical timing of the resulting tradeoffs. In agreement with the differences predicted by Core *cMR* models (Figure 7), we found opposite directions of evolution between *cMR.80lvr* and body size, both between Haplorhini and Glires, as well as within each clade (Figure 8).

Among primates, an accelerated increase in liver *cMR* accompanied the decrease in size of two of the smallest Platyrrhini, one of which (*Callithrix pygmaea*) may be heterothermic[60]. A clade of five small (< 1.0 kg) Platyrrhini exhibited an accelerated *decrease* in brain *cMR.70* paired with elevated levels of *cMR.80lvr*, consistent with adaptation to a low energy regime and greater reliance on gluconeogenesis. The evolution of brain *cMR.70* appeared arrested in Glires and Strepsirrhini relative to Haplorhini, and those species that underwent the most severe reduction in size exhibited the greatest increases in liver *cMR.80*; conversely, the largest species among Glires (Lagomorpha) exhibited the lowest liver *cMR*s (Figure 8).

Brain *cMR.70* increased in intensity and its rate of evolution accelerated with the divergence of Haplorhini, and again with that of humans, in contrast to its relative stasis or decrease among Glires, Lemuriformes and smaller Platyrrhini (Figure 8). The relative levels of heart *cMR.70* generally tracked body size, with accelerated rates of heart evolution in the clades of the largest Glires (Lagomorpha) and primates (Catarrhini). The divergence of humans was marked by an exceptional increase in the rate of evolution of the cMR.70 of the kidney, as well as that of the brain (Figure 8).

DISCUSSION

The inference of cellular metabolic rates

Venditti et al (2024) recently questioned the interpretation of the conventional index of mammalian brain size evolution, the slope of log *Mbrn versus* log *Mbdy*, noting a curvilinear relationship with body size, independent of phylogeny[23]. Moreover, it is readily demonstrable that this index does not reflect the relative energy consumption of the brain (*rMRbrn*/*rMRbdy*), a more immediate and sensitive target of selection than either log-transformed brain size or body size, *per se* (Figure 9).

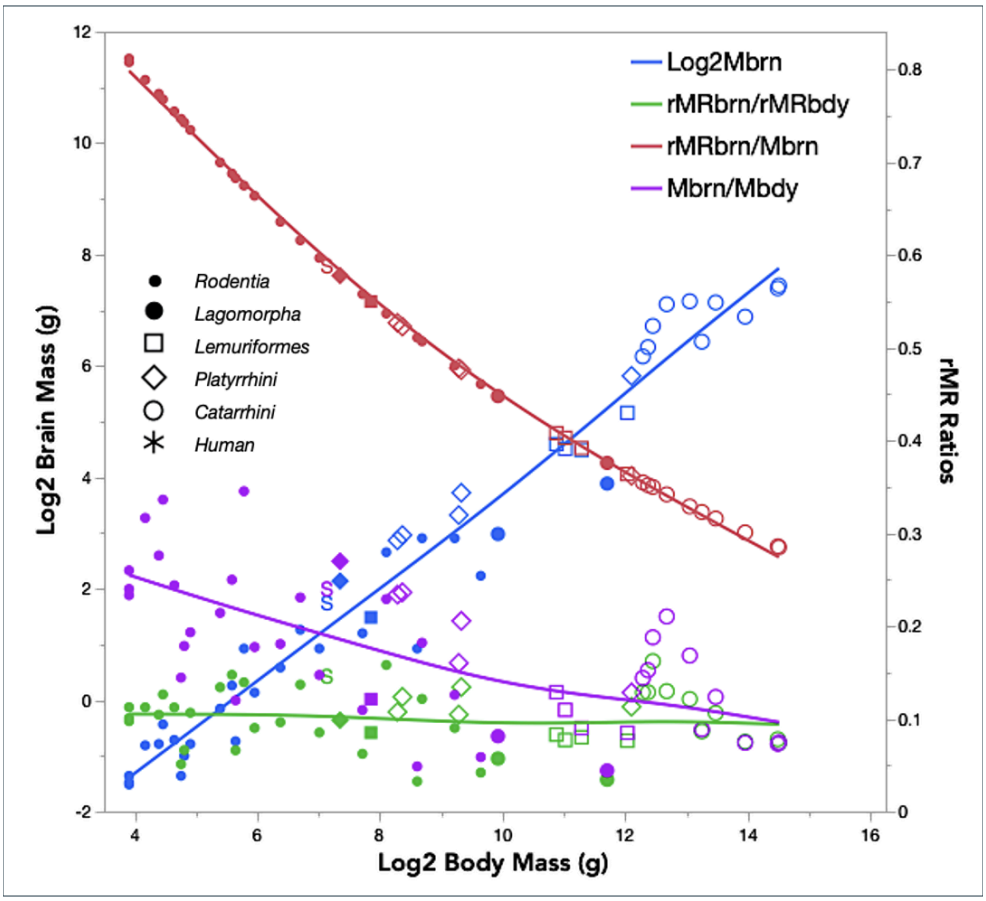

Figure 9. Fundamental relationships among brain and body size and rates of energy consumption. Euarchontoglires include 22 primates and a Scandentia (S). Filled rectangle, diamond = heterotherm.

- The ratio *Mbrn*/*Mbdy decreases* with size, contrary to the slope of log *Mbrn versus* log *Mbdy* (R^2 = 0.42 overall, 0.53 among 26 Glires P = 1.60e-05).
- The relative energy consumption of the brain, *rMRbrn*/*rMRbdy*, is weakly dependent on size, but only among Glires (R^2 = 0.16, P = 2.57e-02).
- The ratio *rMRbrn*/*Mbrn decreases* as a quadratic function of body mass, consistent with surface area considerations (R^2 = 1.00, P = 0.00). All data were drawn from Wang et al (2012)[56].

The conventional power law model allows the *rMR*s of species varying in mass over several orders of magnitude to be made a linear function of *M* by log transformation, regardless of phylogenetic order[54]. Phylogenetic comparative methods can then be applied to deconvolve inherited variation from variation that is random or adaptive[50-51]. However, mass-corrected *MR* ($rMRbdy/Mbdy^{0.75}$) ranges only twofold across mammals, and the physical and ecological factors to which organ and body *rMR*s have adapted, notably temperature and the availability of water, vary even less. Unlike the fixed *sMR* value derived from the slope of log *rMRorg*/log*Morg*, a distribution of *cMR*s can be matched to the distribution of a relevant physiological or thermodynamic variable without log transformation, yielding a homoscedastic regression amenable to phylogenetic comparative analysis[9].

The choice between *sMR* and *cMR* then reflects an assumption regarding the nature of metabolic allometry in homeotherms: whether it reflects the indirect outcome of correlational selection on the individual variables mass and *rMR* (White et al, 2019)[62], or else the outcome of direct selection on the rates of heat generation and dissipation. Consistent with the latter model, mammalian *cMR*s are sensitive to body temperature and robust to variation in the range of body mass, unlike *sMR*s[9].

Thermoregulatory* versus *developmental constraints on organ size

Since the seminal analysis by Lande (1979)[43], it has been the convention to base the allometry of brain size on whole body mass[63-64]. This approach has not detected significant anticorrelations among organ sizes[18], perhaps not surprisingly, given that organ sizes are developmentally programmed to track body mass[65]. We have previously shown in mammals that a model of stabilizing selection accounted better for the dependence on *mirFam* of whole-body *cMR* than did a Brownian motion process[9], with an optimal *cMR* scaling of $M^{0.75}$. In the present study, this corresponds to the zone of minimal constraint by body size on the composition of the 4-organ Core. Moreover, additive models of both *cMR.75cor* and *sMR.75cor* were dependent only on the *cMR* of the liver, implying a degree of uncoupling of thermogenic organ mass from body size. The observation that only the dependence of *cMR.80lvr* on body size remained unchanged across clades suggests a hierarchy of organ size regulation: *across clades*, liver size and activity have been developmentally programmed to track body size, which varies geometrically; *within clades*, thermal homeostasis has been maintained by adjusting the relative proportions of the other thermogenic organs, in response to factors that vary arithmetically.

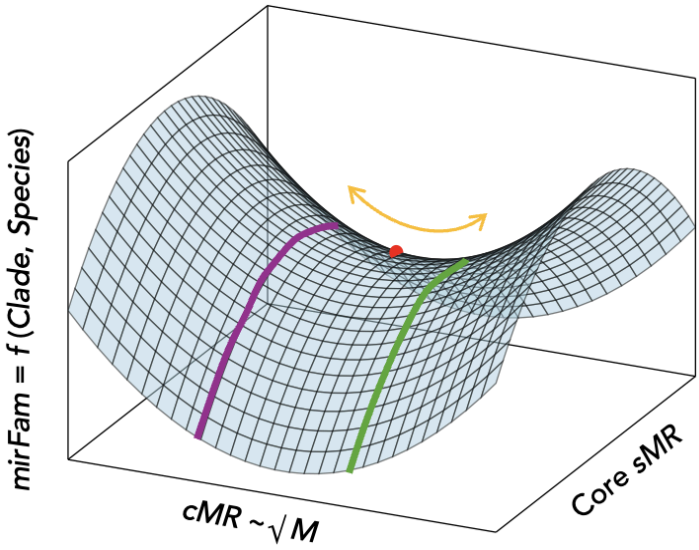

.

Figure 10. *mirFam*-based organ *cMR*s are displaced from the zone of minimal mass dependence defined by the Core *sMR*. Brain (purple) and liver (green) *cMR*s exhibit opposite patterns of correlation with body size.

Figure 10 depicts the relationship between organ *cMR*s and Core *sMR* as a function of the evolution of the number of microRNA families. The clade-wide expansions of the microRNA-target apparatus that have accompanied major increases in metabolic rates may have served to maintain metabolic efficiency by limiting the expression noise associated with faster rates of protein synthesis[66], driver of 20% of ATP turnover in mammalian cells[67]:

a) the interactions between microRNAs and targeted messenger RNAs constitute a well-established mechanism to attenuate intrinsic translation noise[68-69], preferentially repressing the translation of low-abundance transcripts[70];
b) the distributions of the rates of translation of low- and high-abundance mRNAs appear to have evolved under an energy efficiency constraint[71] and conform to the predicted outcome of global activity of microRNAs[70], which can be understood in the light of the 10- to 100-fold higher thermodynamic cost per gene of translation, relative to transcription, in eukaryotes[72-73].

Thus, the saddle function may also be interpreted as an energy efficiency/fitness landscape (Figure 9).

Lande (1979) attributed the enlargement of brain size in primates *versus* Glires to a genetic uncoupling of its dependence on body size[44]. Our thermodynamic models of Core *cMR* in carnivores, primates and Glires, together with Bayesian reconstruction of the evolutionary tradeoff between between liver and brain *cMR*s, suggest an inversion of this premise, namely, a disproportionate reduction of body size relative to brain size upon the divergence of Glires from primates, and Platyrrhini from Catarrhini (see Smaers et al, 2021 for a similar interpretation[64]). Consequently, average *Mbrn*/*Mbdy* ratios in Glires and Platyrrhini have remained significantly *higher* than the ratios in primates and non-human Catarrhini, respectively, in both cases contrary to the rank order of the ratio log *Mbrn*/log *Mbdy* (Supplementary Table S3). These examples further illustrate how log ratios invert the rank order of the ratios of untransformed trait values, leading to different interpretations of evolutionary change.

The developmental and phylogenetic plasticity of the liver

Of the six possible *cMR* tradeoffs among four thermogenic organs, the brain - liver tradeoff is the most significant and most highly conserved. Since we detected the brain - liver tradeoff among all clades of Theria that we examined, this plasticity appears to be an inherent property of the mammalian evolutionary toolkit, not limited to homeotherms. Upon depletion of glycogen in the fasting state, the liver serves as the primary organ of gluconeogenesis: the glucagon-dependent reduction of amino acid or glycerol carbons, fueled by free fatty acids released from adipose tissue. Gluconeogenesis

contributes 40 - 60% of total glucose production after an overnight fast in humans, and greater than 90% after 48 hours of fasting[74]. Liver oxidation of fatty acids also generates ketone bodies that provide 60% of the human brain's energy during a prolonged fast, thereby sparing muscle protein[75]. Elevated levels of circulating fatty acids induce insulin resistance in liver and skeletal muscle[75], an additional mechanism to ensure an uninterrupted supply of glucose to the brain which, unlike these organs, cannot switch to fatty acid oxidation. Interestingly, specific microRNAs have been found to regulate many of the effectors mediating the transition between the fed state/lipogenesis and the fasting state/lipolysis[76-78].

Brain glucose utilization peaks around age five in humans, early in the extended period between weaning and sexual maturity, which is also the period of slowest growth in body mass[79]. Based on the turnover of isotopically-labeled glucose, glucose production was proportional to brain mass over the entire lifespan, and therefore highest among young children[80]. Among prepubertal children (7 - 9 years of age), the rate of gluconeogenesis was still 50% higher than that found among adolescents[81-82]. The inverse relationship between developmental changes in the brain's glucose uptake and the rate of body mass growth[79] implicate the liver as the pivotal partner in this ontogenetic tradeoff.

Drawing on metabolite fluxes measured in humans, a computational model of the equivalent fluxes in mice found that following an overnight fast, the rates of liver gluconeogenesis, lipolysis and proteolysis were all elevated ~ 10-fold in mice, compared to the corresponding rates in humans[83]. These findings comport well with the opposite directions of evolution of *cMR.80lvr* that we found between Glires and primates, which are associated with divergent body size and life history strategies, notably population turnover[84-86]. The apparent evolutionary plasticity of the liver appears to have co-opted the liver's inherent mechanism of developmental plasticity: among mammalian organs, only the liver retains full regenerative potential[65]. If the evolution of liver size has adapted to both thermoregulatory constraints and the demand for glucose production, then a situation of high energy reliability/low dependence on gluconeogenesis in an incipient clade may have favored reductions in relative liver size and/or thermogenesis, such as those associated with the divergences of Lagomorpha and Catarrhini. Conversely, smaller bodies and a tradeoff favoring the liver appear to signify adaptation to limited energy resources relative to population size, as exemplified by the divergence of Glires from Euarchontoglires, Strepsirrhini from primates, and Platyrrhini from Haplorhini.

Hippo-YAP, the bilaterian regulator of organ size[87], coordinates liver growth with the suppression of

gluconeogenesis[88-91]. Significantly, the global underexpression of microRNAs that is frequently observed in tumor cells has been attributed to aberrant density-dependent regulation of the same Hippo-YAP signaling[92]: at low cell densities, Hippo signaling is normally suppressed, allowing YAP to localize in the nucleus and stimulate cellular proliferation, while at normal organ size and tissue density, YAP translocation and activity are inhibited by Hippo[87]. Constitutively active YAP suppresses microRNA levels in cells and tumors and post-transcriptionally induces oncogenic MYC protein[92-93]. Any resulting alteration in microRNA levels would be expected to cause dysregulation of gene regulatory networks (GRNs), either by disrupting the timing of transient signals, such as transcription factors[94-95], or else by shifting of the repression profile of targets regulated by multiple microRNAs[70]. By extension, the evolutionary plasticity of the liver implies a resetting of the dynamic ranges for the interactions among Hippo-YAP signaling, organ size, and the rate of microRNA biogenesis.

A feedback model for brain size and energy reliability

We modeled a simple feedback loop based on the association of larger brain size and *mirFam* with declining rates of liver thermogenesis, assuming that these reflect decreasing dependence on gluconeogenesis: energy reliability facilitates an increase in brain size which, in turn, facilitates improved energy reliability up to the limits imposed by anatomy and physiology, such as the diameter of the birth canal, or the physiological limit on the rate of heat dissipation[10]. Since the emergence of permanent homeothermy among Boreoeutheria was associated with a clade-wide increase in *mirFam*[9], we assigned *mirFam* to serve as a proxy for energy reliability. Using a logistic function, we fit *mirFam* to the primate brain size dataset of Grabowski et al (2023)[12]:

$$\frac{d\,(mirFam)}{d\,(\log V_{brn}/\log M_{bdy})} = r \bullet mirFam\,(1 - mirFam/mirFam_{max}),$$

where ***r*** is the growth rate, and the range of *mirFam* has been scaled to a range of 1.0.

As shown in Figure 11-A, log *Mbrn*/log *Mbdy* is a predictor of *mirFam,* rather than the converse, consistent with the proposition that evolutionary increases in brain size were associated with greater energy reliability. Since *mirFam* can also be fit to the relative sizes of the other thermogenic organs, the question arose as to which relationship might be the principal target of selection. The ranges of *mirFam* are highly clade-specific (Supplementary Figure S6); hence *mirFam* variation with respect to

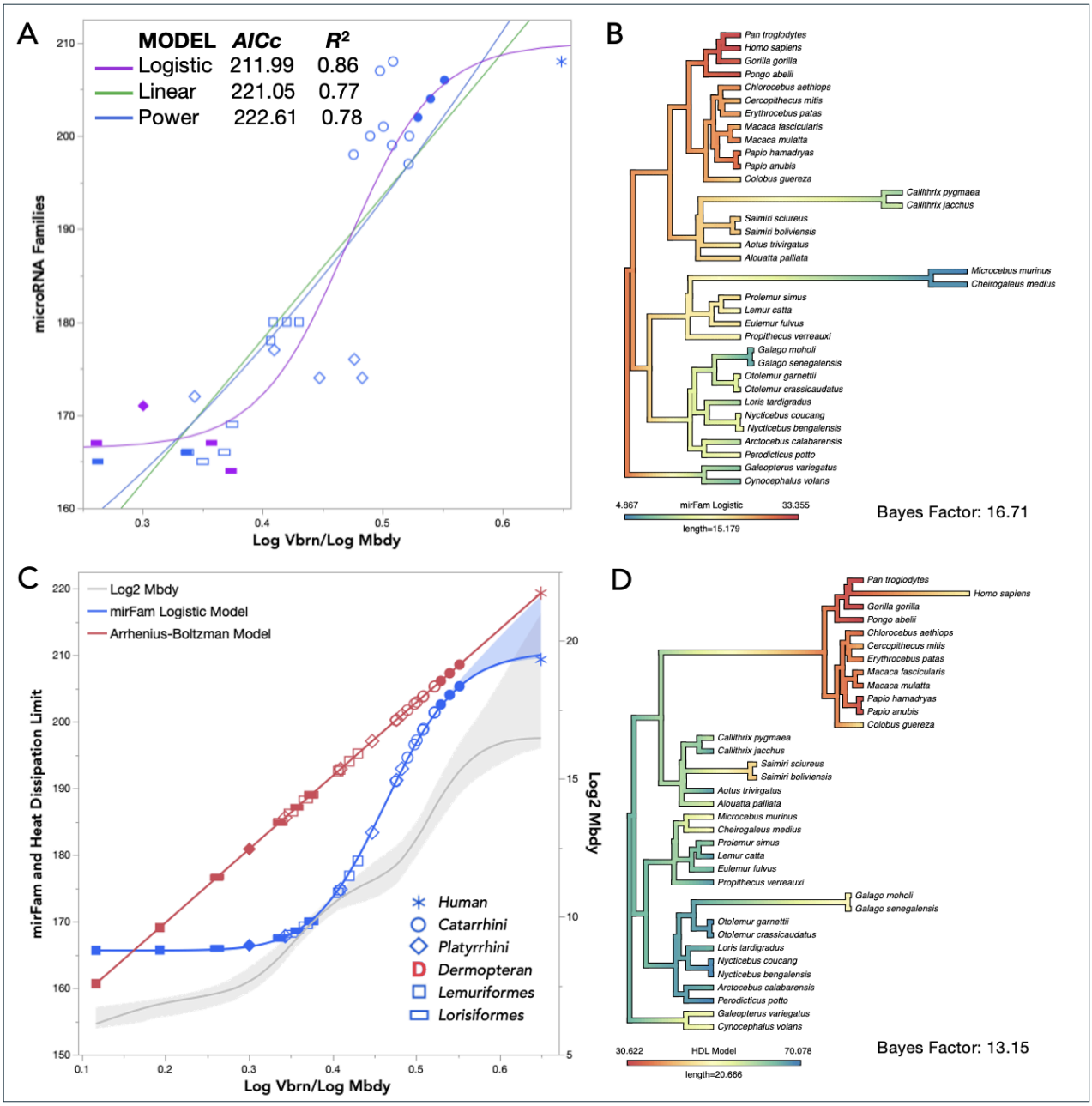

Figure 11. Logistic model of the *mirFam* relationship to relative brain size and the primate heat dissipation limit.
A. A logistic model of *mirFam* variation with respect to Log*Vbrn*/Log*Mbdy* was compared with linear and power law models. Filled symbols: circles = Hominidae; rectangles and diamond: documented (blue) and suspected (purple) heterotherms. The model was generated without heterotherms *M. murinus* and *C. medius* (*N* = 31).
B. Variable rate phenogram based on the linearized values of the logistic model: when ranked in ascending order, the ratios of model *mirFam* values to the cumulative sum decrease in a linear manner[96]. Dummy values were added to either end of the range of predicted values in order to ensure linearity across the range of *mirFam*.
C. Comparison of the logistic model with the maximal rate of thermogenesis predicted from whole-body mass and T_b[97] and scaled to the same range as *mirFam*. Shading represents the confidence interval (spline method).
D. The number of microRNA families predicted by the logistic model were subtracted from the number predicted by the heat dissipation model and the resulting distribution as centered. In order to detect the adaptive changes shown it was necessary to exclude the outlier clade of dwarf and mouse lemurs (Cheirogaleidae) (see panel A).

any trait is always secondary to phylogenetic distance. However, in phylogenetic regressions on *mirFam*, all potential kidney and heart *cMR*s (*cMR.60* - *cMR.80*) varied independently of phylogenetic distance (Pagel's *lambda* = 0.0), as did all but one liver *cMR* (*cMR.60lvr*) (Supplementary Table S4). In contrast, brain *cMR* variation with respect to *mirFam* was, in every case, secondary to phylogenetic distance (*lambda* = 1.0). Thus, the divergence of primate clades coincided specifically with changes in the dynamic range of *mirFam* with respect to *cMR.70brn*.

A variable rate phenogram corresponding to this logistic model was generated using the ratios from the Hubbert linearization of the logistic function (Figure 11-B)[96], so that the color scale reflects rank order. The three smallest-bodied clades, *Cheirogaleidae, Galago and Callithrix* (marmosets) exhibited an accelerated descent in rank. The latter observation is consistent with the apparent regression of the brain size allometry of Callitrichines, more similar to that of Strepsirrhini than of Platyrrhini[64]. *Callithrix pygmaea* may also be heterothermic[60], and the *Callithrix* clade also exhibited marked increases in the level and rate of evolution of liver *cMR.80*, suggesting adaptation to a regime of minimal energy reliability, perhaps related to low calorie-density folivory or insectivory[98]. In sum, the *mirFam*-based logistic model implies that size reduction has been a consistent adaptation to low energy reliability.

Extending this logic, we postulated that the upper plateau of the logistic model, occupied by primates with the largest bodies and relative brain sizes corresponds to a physiological limit on the rate of heat dissipation[10]. This interpretation is supported by the observation that when primate species are ranked by size, *mirFam* varies reciprocally with the Arrhenius function, $1/T_b$ (ºK) (Supplementary Figure S7). Thus, the seemingly random variation in T_b within each clade is actually tied to the variation in *mirFam*, except among small heterotherms (Supplementary Figure S7). The conserved nature of this relationship lends itself to the following formulation of a maximum heat dissipation limit (HDL). The relationship between whole body *rMR* and T_b can be described by the Arrhenius-Boltzmann function, $e^{-E/kT}$, where E represents the mean activation energy of the respiratory complexes and k is the Boltzmann constant[97]. When corrected for whole-body mass, this function (B/B_0) represents the maximal theoretical rate of thermogenesis, and therefore of heat dissipation, regardless of phylogeny or thermoregulatory adaptations (Figure 11-C).

In order to detect adaptation that occurred in relation to this limit, we generated variable rate phenograms that traced the direction and rate of evolution of the *difference* between the predictions of

the HDL model and the logistic model (Figure 11-C). In this case, the color scale reflects proximity to the HDL. Interestingly, two of the clades that exhibited accelerated evolution toward the HDL represented the highest relative brain size among Platyrrhini (*Saimiri*) and lowest relative brain size among Lorisiformes (*Galago*), suggesting a thermoregulatory cost at the extremes of variation (Figure 11-D) (Supplementary Table S2). The divergence of Catarrhini was associated with accelerated evolution toward the HDL that reversed with the subsequent divergence of the human and colobus monkey, clades that again represent the extremes of relative brain size within their clade (Catarrhini) (Figure 10-D). The marked "cooling" in the case of the human reconciles the disproportionate increase in brain size with our species' unique adaptations for heat dissipation (Figure 11-D).

Our logistic model assigns the ancestral primate a high rank for energy reliability and a low rank relative to the HDL, a propitious combination for the founder of a new order of mammals in a new fitness landscape[99]. In many respects this model, derived from the reparametrization of rates of organ energy consumption in terms of *mirFam*-based *cMR*s, fulfills the recent call for an explanation of the distinct pattern of brain size evolution in primates "in terms of the release of a constraint or an adaptive shift that initiated escalating feedback between brain and behavior"[23]. Together with the underlying Core model of thermoregulation[44], it has allowed us to uncover a conserved energy tradeoff that was first proposed four decades ago in order to account for the expansion of brain size in the human lineage[41-42]. Since this logistic model is agnostic regarding underlying mechanisms, it may also serve as a null hypothesis for comparison with the evolution of candidate mechanisms of adaptation.

Implications for evolutionary medicine

The reparametrization of *cMR*s also has far-reaching implications for evolutionary medicine[100]. For example, human kidney *cMR.70* underwent an adaptive increase to a level 30% higher than that found in other hominoid apes; by comparison, the value for the human was 10% *lower* when scaled according to the slope (0.90) of log *rMRkdn*/log *Mkdn*. Since the kidney is responsible for the homeostasis of pH, nitrogen, sodium, water and glucose, the rapid evolution *cMR.70kdn* in humans may represent adaptation to a diet enriched in lipid and protein[14-15], or to an altered landscape of opportunities for hydration *versus* risks of dehydration ("Savanna hypothesis")[25-27]. As it is, the kidneys of modern humans are quite susceptible to damage by heat stress: exposure to 40ºC for as little as one hour is sufficient to redirect blood flow to the skin, reduce blood flow to the kidney by one third[101] and trigger responses promoting water conservation that can eventually lead to acute kidney injury,

such as activation of the renin-angiotensin-aldosterone system[102-103]. Since the ability to thermoregulate is highly dependent on water balance, ancestral humans may have been even more vulnerable to kidney damage and hyperthermia prior to the adaptive increase in *cMR.70kdn*, linked to dehydration. Baboons are diurnally active and their fossils appear in the same arid horizons as the fossils of *Australopithecus*[104] and *Homo*[26]. When free-ranging baboons were deprived of water and exposed to elevated ambient temperatures they developed a progressive hyperthermia, with core temperature increasing on each day water was withheld, that was rapidly reversed upon rehydration[105].

It is not generally appreciated[106] that maintenance of temperature homeostasis and water balance may have driven another uniquely human adaptation, the remarkable ability to store fat: adipose tissue was found to make up 41% of the body mass in adult women, compared to 9% in chimpanzee and 14% in gorilla females[19]. In addition to a prolonged the ability to release fatty acids, thereby sparing glucose for the brain, fatty acid oxidation generates a high molar ratio of water, which may appreciably affect overall water balance[107]: rats fed a high fat diet consumed less water following deprivation[108], and men who are obese manifested diminished thirst in response to dehydration[109]. Camels[110] and fat-tailed sheep[111] represent two other genera that manifest excess adiposity, relative to non-desert adapted ungulates. Along with studies of aboriginal populations inhabiting the same arid regions for thousands of years, evidence of more rapid evolution and differential expression has been found among desert-adapted mammals for genes or gene families mediating lipid metabolism, insulin responsiveness, water and solute transport, as well as the activity of renin-angiotensin-aldosterone complex[112]. The permanent enlargement of breast tissue, in addition to providing nutrition during the extended infancy of humans[17], may have also served a thermoregulatory function in a savanna environment that was hotter by day and cooler by night[113-114], as well as a portable buffer against infant dehydration. In sum, detection of the adaptive increase in human kidney *cMR* in the ancestors of modern humans prompts a reappraisal of uniquely human adaptations associated with the transition to a savanna ecosystem related to water and temperature homeostasis.

SYNTHESIS

The adaptive value of repression by individual microRNAs operating in gene regulatory networks has been attributed to their ability to canalize phenotype expression by buffering the effects of environmental or allelic variation[115-116], to set thresholds for cell fate determination, and to maintain the identity of differentiated cells by defining ranges of protein expression[117-118]. Major stages in the

diversification of animal cell types, morphologies and complexity of behavior have corresponded to significant expansions of microRNA and target repertoires[119-123]. For example, the emergence of placental mammals is marked by the appearance of 13 novel implantation-related microRNA families[124], and the cognitive success of the genus *Octopus* has been linked to 34 novel microRNA families that are preferentially expressed in neural tissues[125]. However, these *post hoc* associations do not shed light on the conditions of repertoire expansion, nor on the relationship between new or enhanced traits and the increase in *mirFam*, as opposed to action of individual new microRNAs[119].

The emergence of permanent homeothermy in the ancestral clade of Boreoeutheria and the attendant acceleration of metabolic rates was accompanied by a 15% expansion of the number of microRNA families[9], consistent with evidence that microRNAs are required to synchronize the timing of transient signals with metabolic rates[94-95]. A similar *mirFam* expansion accompanied the divergence of Catarrhini: in this study, we have been able to chart *mirFam* as a function of relative brain size, without reference to phylogeny, and link it to a reciprocal decline in thermogenesis by the liver, the primary organ of gluconeogenesis. These observations suggest that a high level of energy reliability, and presumably fitness, in an incipient clade may be a precondition for a significant expansion of the microRNA repertoire. What appear in the evolutionary record as clade-wide shifts to a higher number of microRNA families[49] and higher density of conserved target sites[9], would have necessitated a global reset of the dynamic ranges of microRNAs with respect to effector pathways and the repression profiles of targets that are regulated by multiple microRNAs[70]. Although steady-state microRNA levels are stabilized by numerous homeostatic mechanisms[124-131], the robustness of such GRNs could have, in theory, facilitated rather than impeded the emergence of new or enhanced phenotypes[132-134]. The two examples associated with microRNA repertoire expansion that we have considered here, the emergence of permanent homeothermy and the increase brain size in Catarrhini, together with the observation that *mirFam* losses have occurred much less frequently than gains[135], suggest the operation of a ratchet mechanism that selects among novel candidate microRNAs those that confer greater energy reliability. An analogy may be drawn to the fate of duplicated genes of transcription factors (TFs): owing to their established specificities, they are much more likely to be retained than the paralogues of non-TF genes[136]. Another avenue of investigation, amenable to animal experimentation, is the reciprocal variation of liver size and activity with those of the other Core organs, echoing the developmental tradeoff between the rate of gluconeogenesis and the rate of somatic growth in humans[79]. The nature of the setpoint for organ size relative to body size in mammals is still largely

unexplained[65], much less any mechanism that might account for the evolutionarily conserved tradeoffs between embryologically distinct Core organs[137]. However, we note that organ growth rates *in utero* must be synchronized by a sequence of transient signals, the timing of which is likely to depend on the microRNA milieu.

DECLARATIONS

Limitations

The three principal limitations of this study are:

i) the indirect origin of the mammalian organ *rMR*s: other than one set of *in vivo* measurements in humans[3], these have been inferred from organ masses assuming allometric scaling inferred from humans[4], rats, rabbits, cats and dogs (for additional references, see Wang et al 2012[1]).

ii) the small number and variable quality of the body temperature data in the AnAge database[9];

iii) underestimates of the number of conserved microRNA families by the MirMachine algorithm[10], relative to the reference, manually-curated database[11] (currently MirGeneDB 3.0).

These factors are not expected to affect the qualitative interpretation of our results.

Data Availability

All original data with accompanying references are provided in Supplementary Tables S1 - S4.

Acknowledgment

BF is supported by the Tromsø forskningsstiftelse (TFS) [20_SG_BF 'MIRevolution'].

Author Contributions

Conceptualization: TS; Methodology: TS; Investigation: BF and TS; Writing – Original Draft: TS; Writing – Review & Editing: BF and TS; Visualization: TS; Funding Acquisition: BF.

Declaration of Interests

The authors declare no competing interests.

Statement on the use of AI

No part of this work was generated or edited using AI.

REFERENCES

1. Baker J, Meade A, Pagel M and Venditti C. 2015. Adaptive evolution toward larger size in mammals. *Proc Natl Acad Sci USA* **112**: 5093-5098.

2. Avaria-Llautureo J, Hernandez CE, Rodriguez-Serrano E and Venditti, C. 2019. The decoupled nature of basal metabolic rate and body temperature in endotherm evolution. *Nature* **572**: 651-654.

3. Naya DE, Spangenberg L, Naya H and Bozinovic F. 2013. Thermal conductance and basal metabolic rate are part of a coordinated system for heat transfer regulation. *Proc Roy Soc B* **280**: 20131629.

4. Fristoe TS, Burger JR, Balk MA, Khaliq I, Hof C and Brown JH. 2015. Metabolic heat production and thermal conductance are mass-independent adaptations to thermal environment in birds and mammals. *Proc Natl Acad Sci USA* **112**: 15934-15939.

5. Araújo MB, Ferri-Yáñez F, Bozinovic F, Marquet PA, Valladares F and Chown SL. 2013. Heat freezes niche evolution. *Ecol Letters* **16**: 1206-1219.

6. Khaliq I, Hof C, Prinzinger R, Böhning-Gaese K and Pfenninger M. 2014. Global variation in thermal tolerances and vulnerability of endotherms to climate change. *Proc Roy Soc B* **281**: 20141097.

7. Bennett JM, Sunday J, Calosi P, Villalobos F, Martínez B, Molina-Venegas R, Araújo MB, Algar AC, Clusella-Trulas S, Hawkins BA, Keith SA, Kühn I, Rahbek C, Rodríguez L, Singer A, Morales-Castilla I and Olalla-Tárraga MA. 2021. The evolution of critical thermal limits of life on Earth. *Nature Comm* **12**: 1198.

8. Clarke A, Rothery P and Isaac NJ. 2010. Scaling of basal metabolic rate with body mass and temperature in mammals. *J Anim Ecol* **79**: 610–619.

9. Fromm B and Sorger T. 2023. Rapid adaptation of cellular metabolic rate to the microRNA complements of mammals and its relevance to the evolution of endothermy. *iScience* **27**: 108740.

10. Speakman JR and Król E. 2010. Maximal heat dissipation capacity and hyperthermia risk: neglected key factors in the ecology of endotherms. *J Anim Ecol* **79**: 726-746.

11. Kuderna LFK, Gao H, Janiak MC . . (many others) . . Bonet TM. 2023. A global catalog of whole-genome diversity from 233 primate species. *Science* **380**: 9-913.

12. Grabowski M, Kopperud BT, Tsuboi M and Hansen TF. 2023. Both diet and sociality affect primate brain-size evolution. *Syst Biol* **72**: 404-418.

13. Yegian AK, Heymsfield SB, Castillo ER, Müller MJ, Redman LM and Lieberman DE. 2024. Metabolic scaling, energy allocation tradeoffs, and the evolution of humans' unique metabolism. *Proc Natl Acad Sci* 121: e2409674121

14. Simmen B, Pasquet P, Masi S, Koppert GJA, Wells JCK and Hladik CM. 2017. Primate energy input and the evolutionary transition to energy-dense diets in humans. *Proc Roy Soc B* **284**: 20170577.

15. Paine OCC, Koppa A, Henry AG . . (many others) . . Sponheimer M. 2019. Seasonal and habitat effects on the nutritional properties of savanna vegetation: Potential implications for early hominin dietary ecology. *J Hum Evol* **133**: 99-107.

16. Zeller E, Timmermann A, Yun KY, Raia P, Stein K and Ruan J. 2023. Human adaptation to diverse biomes over the past 3 million years. *Science* **380**: 604 - 608.

17. Mascia-Lees FE, Relethford JH and Sorger T. 1986. Perspectives on permanent breast enlargement in human females. *Amer Anthro* **88**: 423-428.

18. Navarette A, van Schaik CP and Isler K. 2011. Energetics and the evolution of human brain size. *Nature* **480**: 91-93.

19. Pontzer H, Brown MH, Raichlen DA . . (many others) . . Ross SR. 2016. Metabolic acceleration and the evolution of human brain size and life history. *Nature* **533**: 390-393.

20. Martin RD. 1996. Scaling of the mammalian brain: the maternal energy hypothesis. *Physiology* **11**: 149-156.

21. Isler K and van Schaik CP. 2012. Allomaternal care, life history and brain size evolution in mammals. *J Human Evol* **63**: 52-63.

22. Heldstab SA, Isler K, Graber SM, Schuppli C and van Schaik. 2022. The economics of brain size evolution in vertebrates. *Curr Biol* **32**: R697-R708.

23. Venditti, C, Baker J and Barton RA. 2024. Co-evolutionary dynamics of mammalian brain and body size. *Nat Ecol Evol* **8**: 1534–1542.

24. Timmermann A, Yun KS, Raia P . . (many others) . . Ganopolski. 2022. Climate effects on archaic human habitats and species succession. *Nature* **604**: 495-501.

25. Dart, RA. *Australopithecus africanus*: the man–ape of South Africa. 1925. *Nature* **115**: 195-199.

26. Reed KE. Early hominid evolution and ecological change through the African Plio-Pleistocene. 1997. *J Hum Evol* **32**: 289-322.

27. Davies TJ, Daru BH, Bezeng BS . . (many others) . . Bond WJ. 2020. Savanna tree evolutionary ages inform the reconstruction of the paleoenvironment of our hominin ancestors. *Sci Rep* **10**: 12430.

28. Kamberova YG, Guhana SM, DeMarchisa A, Jianga J, Wright SS, Morgan BA, Sabetid PC, Tabina CJ, and Lieberman DE. 2018. Comparative evidence for the independent evolution of hair and sweat gland traits in primates. *J Hum Evol* **125**: 99–105.

29. Morin E and Winterhalder B. 2024. Ethnography and ethnohistory support the efficiency of hunting through endurance running in humans. *Nature Hum Behav* **8**: 1065-1075.

30. Hora M, Pontzer H, Wall-Scheffler CM and Sládek V. 2020. Dehydration and persistence hunting in *Homo erectus*. *J Hum Evol* **138**:102682.

31. Magalhães JP, Abidi Z, dos Santos GA . . (many others) . . Ka Po To P. 2024. Human Ageing Genomic Resources: updates on key databases in ageing research. *Nucl Acids Res* **52**: D900-D908.

32. Lassen NA. 1985. Normal average value of cerebral blood flow in younger adults is 50 ml/100 g/min. *J Cereb Blood Flow Metab* **5**: 347-349.

33. Claassen JAHR, Thijssen DHJ, Panerai RB and Faraci FM. 2021. Regulation of cerebral blood flow in humans: physiology and clinical implications of autoregulation. *Physiol Rev* **101**: 1487-1559.

34. Wang H, Wang B, Normoyle K, Jackson K, Spitler K, Sharrock MF, Miller CM, Best C, Llano D and Du R. 2014. Brain temperature and its fundamental properties: a review for clinical neuroscientists. *Front Neurosci* **307**: 1-17.

35. Nybo L. Brain temperature and exercise performance. 2012. *Exp Physiol* **97**: 333-339.

36. Jessen C, Laburn HP, Knight MH, Kuhnen G, Goelst K, and Mitchell D. 1994. Blood and brain temperatures of free-ranging black wildebeest in their natural environment. *Am J Physiol* 267: R1528–R1536.

37. Mitchell D, Maloney SK, Jessen C, Laburn HP, Kamerman PR, Mitchell G and Fuller A. 2002. Adaptive heterothermy and selective brain cooling in arid-zone mammals. *Comp Biochem Physiol B* 131: 571-585.

38. Yablonskiy DA, Ackerman JJH and Raichle MR. 2000. Coupling between changes in human brain temperature and oxidative metabolism during prolonged visual stimulation. *Proc Natl Acad Sci USA* **97**: 7603-7608.

39. Leithner C and Royl G. 2014. The oxygen paradox of neurovascular coupling. *J Cereb Blood Flow Metab* **34**: 19-29.

40. Drew PJ. 2022. Neurovascular coupling: motive unknown. *Trends Neurosci* **45**: 809-819.

41. Armstrong E. 1983. Relative brain size and metabolism in mammals. *Science* **220**: 1302-1304.

42. Aiello LC and Wheeler P. 1995. The expensive-tissue hypothesis: the brain and the digestive system in human and primate evolution. *Curr Anthro* **36**: 199-221.

43. Lande R. 1979. Quantitative genetic analysis of multivariate evolution applied to the brain: body size allometry. *Evolution* **33**: 402-416.

44. Porter WP and Kearney M. 2009. Size, shape, and thermal niche of endotherms. *Proc Natl Acad Sci USA* **106**: 19666-19672.

45. Boyles JG, Thompson AB, McKechnie AE, Malan E, Humphries MM and Careau. 2013. A global heterothermic continuum in mammals. *Global Ecol Biogeogr* **22**: 1029-1039.

46. Ruf T and Geiser F. 2015. Daily torpor and hibernation in birds and mammals. *Biol Rev* **90**: 891-926.

47. Clavel J and Morlon H. 2017. Accelerated body size evolution during cold climatic periods in the Cenozoic. *Proc Natl Acad Sci USA* **114**: 4183-4188.

48. Fromm B, Høye E, Domanska D, Zhong X, Aparicio-Puerta E, Ovchinnikov V, Umu SU, Chabot, PJ, Kang W, Aslanzadeh M, Tarbier M, Mármol-Sánchez E, Urgese G, Johansen M, Hovig E, Hackenberg M, Friedländer MR and Peterson KJ. 2022. MirGeneDB 2.1: toward a complete sampling of all major animal phyla. *Nucl Acids Res* **50**: D204-D210.

49. Clarke AW, Høye E, Hembrom AA . . . many others . . . Fromm B. 2025. MirGeneDB 3.0: improved taxonomic sampling, uniform nomenclature of novel conserved microRNA families and updated covariance models. *Nucl Acid Res* **53**: D116–D128.

50. Felsenstein J. 1985. Phylogenies and the comparative method. *Amer Naturalist* **125**: 1-15.

51. Hansen TF. 1997. Stabilizing selection and the comparative analysis of adaptation. *Evolution* **51**: 1341-1351.

52. Pagel M. 1999. Inferring the historical patterns of biological evolution. *Nature* **401**: 877-884.

53. Pagel M, O'Donovan C and Meade A. 2022. General statistical model shows that macro-evolutionary patterns and processes are consistent with Darwinian gradualism. *Nature Comm* **13**: 1113.

54. Kleiber M. Body size and metabolism. 1932. *Hilgardia* **6**: 315-353.

55. Scholander PF, Hock F, Walters V, Johnson F and Irving L. 1950. Heat Regulation in Some Arctic and Tropical Mammals and Birds. *Biol Bull* **99**: 237-258.

56. Wang ZM, Zhang J, Ying Z and Heymsfield SB. Organ-tissue level model of resting energy expenditure across mammals: new insights into Kleiber's Law. 2012. *ISRN Zool*: 673050.

57. de Jong S. SIMPLS: 1993. An alternative approach to partial least squares regression. *Chemometrics and Intelligent Laboratory Systems* **18**: 251-263.

58. Wold S, Johansson E. and Cocchi, M. 1993. PLS: partial least squares projections to latent structures. In *Drug Design: Theory, Methods and Applications* (pp. 523-550). Kluwer ESCOM Science Publisher.

59. Celeux G and Govaert G. Gaussian Parsimonious Clustering Models. 1995. *Pattern Recognition* **28**: 781-793.

60. Tattersall GJ. 2012. Diurnal changes in metabolic rate in pygmy marmosets: Implications for sleep, torpor, and basal metabolism in primates. In: Ruf, T., Bieber, C., Arnold, W., Millesi, E. (eds) *Living in a Seasonal World*, chapter 41: 471-480. Springer.

61. Álvarez-Carretero S, Tamuri A, Battini M, Nascimento F, Carlisle E, Asher R, Yang Z, Donoghue P and Dos Reis M. 2022. A species-level timeline of mammal evolution integrating phylogenomic data. *Nature* **602**: 263-267.

62. White CR, Marshall DJ, Alton LA, Arnold PA, Beaman JE, Bywater CL, Condon C, Crispin TS, Janetzki A, Pirtle E, Winwood-Smith HS, Angilletta MJ, Chenoweth SF, Franklin CE, Franklin CE, Halsey LG, Kearney MR, Portugal SJ and Ortiz-Barrientos D. 2019. The origin and maintenance of metabolic allometry in animals. *Nature Ecol Evol* 3: 598-603.

63. Burger JR, George MA, Leadbetter C and Shaikh F. 2019. The allometry of brain size in mammals. *J Mammal* **100**: 276-283.

64. Smaers JB, Rothman RS, Hudson DR . . (many others) . . Safi K. 2021. The evolution of mammalian brain size. *Sci Adv* **7**: eabe2101.

65. Penzo-Méndez AI and Stanger BZ. 2015. Organ-size regulation in mammals. *Cold Spring Harb Perspect Biol* **7**: a019240.

66. Ozbudak EM, Thattai M, Kurtser I, Grossman AD and van Oudenaarden. 2002. Regulation of noise in the expression of a single gene. *Nature Genetics* **31**: 69-73.

67. Buttgereit F and Brand MD. 1995. A hierarchy of ATP-consuming processes in mammalian cells. *Biochem J* **312**: 163-167.

68. Bartel DP. 2018. Metazoan MicroRNAS. ***Cell*** 173: 20-51.

69. Shang R, Lee S, Seneviratne G and Lai EC. 2023. MicroRNAs in action: biogenesis, function and regulation. *Nat Rev Genet* **24**, 816–833.

70. Schmiedel JM, Klemm SL, Zheng Y, Sahay A, Blüthgen N, Marks DS and van Oudenaarden A. 2015. MicroRNA control of protein expression noise. *Science* **348**: 128-132.

71. Schwanhäusser B, Busse D, Li N, Dittmar G, Schuchhardt J, Wolf J, Chen W and Selbach M. 2011. Global quantification of mammalian gene expression control. *Nature* **473**: 337–342.

72. Wagner A. 2005. Energy Constraints on the evolution of gene expression. *Mol Biol Evol* **22**: 1365–1374.

73. Lynch M and Marinov GK. 2015. The bioenergetic costs of a gene. *PNAS* **112**: 15690-15695.

74. Chung ST, Chacko SK, Sunehag AL and Haymond MW. 2015. Measurements of gluconeogenesis and glycogenolysis: a methodological review. *Diabetes* **64**: 3996-4010.

75. Palmer BF and Clegg DJ. 2021. Starvation ketosis and the kidney. *J Nephrol* **52**: 467-478.

76. Ramírez CM, Goedeke L, Rotllan N, Yoon JH, Cirera-Salinas D, Mattison JA, Suárez Y, de Cabo R, Gorospe M and Fernández-Hernando C. 2013. MicroRNA 33 regulates glucose metabolism. *Mol Cell Biol* **33**: 2891–2902.

77. Agbu P and Carthew RW. 2021. MicroRNA-mediated regulation of glucose and lipid metabolism. *Nature Rev Mol Cell Biol* **22**: 425-438.

78. Price NL, Goedeke L, Suárez Y and Fernández-Hernando C. 2021. miR-33 in cardiometabolic diseases: lessons learned from novel animal models and approaches. *EMBO Mol Med* **13**:e12606.

79. Kuzawa CW, Chugani HT, Grossman LI, Lipovich L, Muzik O, Hof PR, Wildman DE, Sherwood CC, Leonard WR and Lange N. 2021. Metabolic costs and evolutionary implications of human brain development. *Proc Natl Acad Sci USA* **111**: 13010-13015.

80. Bier DM, Leake RD, Haymond MW, Arnold KJ, Gruenke LD, Sperling MA and Kipnis DM. 1977. Measurement of "true" glucose production rates in infancy and childhood with 6,6-Dideuteroglucose. *Diabetes* **25**: 1016-23.

81. Sunehag AL, Treuth MS, Toffolo G, Butte NF, Cobelli C, Bier DM and Haymond MW. 2001. Glucose production, gluconeogenesis, and insulin sensitivity in children and adolescents: an evaluation of their reproducibility. *Ped Res* **50**: 115-123.

82. Sunehag AL, Toffolo G. Treuth MS, Butte NF, Cobelli C, Bier DM and Haymond MW. 2002. Effects of dietary macronutrient content on glucose metabolism in children. *J Clin Endocrinol Metab* **87**: 5168-5178.

83. Kummitha CM, Kalhan SC, Saidel GM and Lai N. 2014. Relating tissue/organ energy expenditure to metabolic fluxes in mouse and human: experimental data integrated with mathematical modeling. *Physiol Rep* **2**: e12159.

84. Jeschke JM, Gabriel W and Kokko H. 2008. r-Strategist/K-Strategists. Jørgensen SE and Fath BD, eds. *Encyclopedia of Ecology*: 3113-3122.

85. Dańko MJ, BurgerO, Argasiński K and Kozłowski J. 2018. Extrinsic mortality can shape life-history traits, including senescence. *Evol Biol* **45**: 395-404.

86. de Vries C, Galipaud M and Kokko H. 2023. Extrinsic mortality and senescence: a guide for the perplexed. *Peer Community Journal* **3**: e29.

87. Camargo FD, Gokhale S, Johnnidis JB, Fu D,1 Bell GW, Jaenisch R, and Brummelkamp TR. 2007. YAP1 increases organ size and expands undifferentiated progenitor cells. *Curr Biol* **17**: 2054-2060.

88. Hu Y Shin DJ, Pan H, Lin Z, Dreyfuss JM, Camargo FD, Miao J, and Biddinger SB. 2017. YAP suppresses gluconeogenic gene expression via PGC1α. *Hepatol* **66**: 2029–2041.

89. Cox AG, Tsomides A, Yimlamai D . . . Goessling W. 2018. Yap regulates glucose utilization and sustains nucleotide synthesis to enable organ growth. *EMBO J* **37**: e100294.

90. Ibar C and Irvine KD. 2020. Integration of Hippo-Yap signaling with metabolism. *Dev Cell* **54**: 256-267.

91. Driskill JH and Pan D. 2021. The Hippo pathway in liver homeostasis and pathophysiology. *Ann Rev Pathol Mech Dis* **16**: 299-322.

92. Mori M, Triboulet R, Mohseni M, Schlegelmilch K, Shrestha K, Camargo FD and Gregory RI. 2014. Hippo signaling regulates Microprocessor and links cell-density-dependent miRNA biogenesis to cancer. *Cell* **156**: 893–906.

93. Zhao B, Wei X, Li W . . . Guan KL. 2007. Inactivation of YAP oncoprotein by the Hippo pathway is involved in cell contact inhibition and tissue growth control. *Genes Dev* **21**: 2747-2761.

94. Cassidy JJ, Bernasek SM, Bakker R, Giri R, Peláez N, Bobrowska A, Bagheri N, Nunes Amaral LA and Carthew RW. 2019. Repressive gene regulation synchronizes development with cellular metabolism. *Cell* **178**: 980-992.

95. Keuls RA, Oh YS, Patel I and Parchem RJ. 2023. Post-transcriptional regulation in cranial neural crest cells expands developmental potential. *Proc Natl Acad Sci USA* **120**: e2212578120.

96. Hubbert MK. 1982. Techniques of prediction as applied to the production of oil and gas. In Gass, Saul I. (ed.) *Oil and Gas Supply Modeling* (proceedings of a symposium held at the Department of Commerce, Washington, DC, June 18–20, 1980). National Bureau of Standards Special Publication **631**: 16-141. Washington (DC).

97. Allen AP, Gillooly JF, Savage VM and Brown JH. 2006. Kinetic effects of temperature on rates of genetic divergence and speciation. *Proc Natl Acad Sci USA* **103**: 9130-9135.

98. Schiel N and Souto A. 2017. The Common Marmoset: an overview of its natural history, ecology and behavior. *Dev Neurobiol* **77**: 244–262.

99. Erwin DH. 2015. Novelty and innovation in the history of life. *Current Biol* **25**: R930-R940.

100. Benton ML, Abraham A, LaBella AL, Abbot P, Rokas A, Capra JA. 2021. The influence of evolutionary history on human health and disease. *Nat Rev Genet* **22**: 269-283.

101. Rowell LB. 1974. Human cardiovascular adjustments exercise and thermal stress. *Physiol Rev* **54**: 75-159.

102. Chapman CL, Johnson BD, Vargas NT, Hostler D, Parker MD, Schlader ZJ. 2020. Both hyperthermia and dehydration during physical work in the heat contribute to the risk of acute kidney injury. *J Appl Physiol* **128**: 715–728.

103. Chapman CL, Johnson BD, Parker MD, Hostler D, Pryor RR and Schlader Z. 2021. Kidney physiology and pathophysiology during heat stress and the modification by exercise dehydration, heat acclimation and aging. *Temperature* **8**: 108-159.

104. Brain CK. 1981. The Hunters or the Hunted?: An Introduction to African Cave Taphonomy. Chicago University Press, Chicago.

105. Brain C and Mitchell D. 1999. Body temperature changes in free-ranging baboons (*Papio hamadryas ursinus*) in the Namib Desert, Namibia. *Intl J Primatol* 20: 585-598.

106. Heldstab SA, van Schaik CP and Isler I. 2016. Being fat and smart:
A comparative analysis of the fat-brain trade-off in mammals. *J Human Evol* **100**: 25-34.

107. Donald J and Pannabecker TL. 2015. Osmoregulation in Desert-Adapted Mammals. In: Hyndman, K, Pannabecker T. (eds) *Sodium and Water Homeostasis*. Physiology in Health and Disease. Springer, New York.

108. Dos-Santos RC, Ishioka G, Cognuck SQ, Mantovani M, Caliman IF, Elias LLK and Antunes-Rodrigues J. 2022. High-fat diet changes the behavioural and hormonal responses to water deprivation in male Wistar rats. *Exp Physiol* **107**: 1454-1466.

109. Chang DC, Stinson EJ, Piaggi P, Krakoff J and Gluck MR. 2023. Disinhibition augments thirst perception from two dehydrating stimuli in men. *Appetite* **182**: 106429.

110. Wu H, Guang X, Al-Fageeh MB, Cao J, Pan S, Zhou H, Zhang L, Abutarboush MH . . (many others) . .
Wang J. 2014. Camelid genomes reveal evolution and adaptation to desert environments. *Nature Comm* **5**: 5188.

111. Xu YX, Wang B, Jing JN, M R, Luo YH, Li X, Yan Z, Liu YJ, Gao L, Ren YL, Li MH and Lv FH. 2023. Whole-body adipose tissue multi-omic analyses reveal molecular mechanisms underlying local adaptation to extreme environments. *Comm Biol* **6**: 159.

112. Rocha JL, Godinho R, Brito JC and Nielsen R. 2021. Life in deserts: the genetic basis of mammalian desert adaptation. *Trends Ecol Evol* **36**: 637-650.

113. Pawłowski B. 1999. Permanent breasts as a side effect of subcutaneous fat tissue increase in human evolution. *Homo J Comp Hum Biol* **50**: 149–162.

114. Pawłowski B and Żelaźniewicz. 2021. The evolution of perennially enlarged breasts in women:
a critical review and a novel hypothesis. *Biol Rev* **96**: 2794-2809.

115. Hornstein H and Shomron N. 2006. Canalization of development by microRNAs.
Nature Genetics **38**: S20-S24.

116. Li X, Cassidy JJ, Reinke CA, Fischboeck S and Carthew RW. 2009. A microRNA imparts robustness against environmental fluctuation during development. *Cell* **137**: 273-282.

117. Mukherji S, Ebert MS, Zheng GXY, Tsang JS, Sharp PA and van Oudenaarden A. 2011.
MicroRNAs can generate thresholds in target gene expression. *Nature Genetics* **43**: 854-859.

118. Ebert MS and Sharp PA. 2012. Roles for MicroRNAs in conferring robustness to biological processes.
Cell **149**: 515-524.

119. Zolboot N, Du JX, Zampa F and Lippi G. 2021. MicroRNAs instruct and maintain cell type diversity in the nervous system. *Front Mol Neurosci* **14**: 646072.

120. Makeyev EV and Maniatis T. 2008. Multilevel Regulation of Gene Expression by MicroRNAs.
Science **319**: 1789-1790.

121. Erwin DH, Laflamme M, Tweedt SM, Sperling EA, Pisani D and Peterson KJ. 2011.
The Cambrian conundrum: early divergence and later ecological success in the early history of animals.
Science **334**: 1091-1097.

122. Dexheimer PJ and Cochella L. 2020. MicroRNAs: from mechanism to organism. *Front Cell Dev Biol* **8**: 409.

123. Peterson KJ, Beavan A, Chabot PJ, McPeek MA, Pisani D, Fromm B and Simakov O. 2022.
MicroRNAs as Indicators into the Causes and Consequences of Whole-Genome Duplication Events.
Mol Biol Evol **39**: msab344.

124. Taylor AS, Tinning H, Ovchinnikov V, Edge J, Smith W, Pullinger AL, Sutton RA, Constantinides B, Wang D, Forbes K, Forde N and O'Connell MJ. 2023. A burst of genomic innovation at the origin of placental mammals mediated embryo implantation. *Comm Biol* **6**:459.

125. Zolotarov G, Fromm B, Legnini I, Ayoub S, Polese G, Maselli V, Chabot PJ, Vinther J, Styfhals S, Seuntjens E, Di Cosmo A, Peterson KJ and Rajewsky N. 2022. MicroRNAs are deeply linked to the emergence of the complex octopus brain. *Sci Adv* **8**: eadd9938.

126. Ghini F, Rubolino C, Climent M, Simeone I, Marzi MJ and Nicassio F. 2018. Endogenous transcripts control miRNA levels and activity in mammalian cells by target-directed miRNA degradation. *Nat Commun* **9**: 3119.

127. Gebert LFR and MacRae IJ. 2019. Regulation of microRNA function in animals.
Nature Rev Mol Cell Biol **20**: 21-37.

128. Sheu-Gruttadauria J, Pawlica P, Klum SM, Wang, S, Yario TA, Schirle Oakdale NT, Steitz JA and MacRae IJ. 2019. Structural Basis for Target-Directed MicroRNA Degradation. *Mol Cell* **75**, 1243–1255.

129. Cui Y, Lu X, Ding L, Ke L, Yang D, Pirouz M, Qi Y, Ong J, Gao G, Du P and Gregory RI. 2021.
Global miRNA dosage control of embryonic germ layer specification. *Nature* **593**: 602-606.

130. Komatsu S, Kita H and Suzuki HI. 2023. Network regulation of microRNA biogenesis and target interaction.
Cells **12**: 306.

131. Hiers NM, Li T, Traugot CM and Xie M. 2024. Target-directed microRNA degradation: Mechanisms, significance, and functional implications. *Wiley Interdiscip Rev RNA* **15**: e1832.

132. Ciliberti S, Martin OC and Wagner A. 2007. Innovation and robustness in complex regulatory gene networks. *Proc Natl Acad Sci* USA **104**: 13591-13596.

133. Barve A and Wagner A. 2013. A latent capacity for evolutionary innovation through exaptation in metabolic systems. *Nature* **500**: 203-206.

134. Catalán P, Wagner A, Manrubia S and Cuesta JA. 2018. Adding levels of complexity enhances robustness and evolvability in a multilevel genotype–phenotype map. *J Royal Soc Interface* **15**: 20170516.

135. Tarver JE, Taylor RS, Puttick MN, Lloyd GT, Pett W, Fromm B, Schirrmeister BE, Pisani D, Peterson KJ and Donoghue PCJ. 2018. Well-annotated microRNAomes do not evidence pervasive miRNA loss. *Genome Biol Evol* **10**: 1457-1470.

136. Baker EA and Woollard A. 2022. The road less travelled? Exploring the nuanced evolutionary consequences of duplicated genes. *Essays in Biochemistry* 66: 737-744.

137. Penzo-Méndez AI and Stanger BZ. 2014. Cell competition in vertebrate organ size regulation. *WIREs Dev Biol* 3: 419-427.

STAR METHODS - *Quantification and Statistical Analysis*

Physiological Data

The masses the four thermogenic organs were obtained from the 111-species dataset of Wang et al (2012)[1], originally derived from the compilation of Navarette et al (2011)[2]. Only in humans have organ metabolic rates been measured directly[3]. Otherwise, they have been inferred by conventional allometric scaling based on organ mass of rat (all four organs), dog (liver, brain and kidney), cat and rabbit (liver)[4]. Relative brain sizes for the logistic models were obtained from Grabowski et al (2023)[5], Smaers et al (2021)[6] (human), and estimated for Dermoptera[7]

Values for thermal conductance (C_{min}) were obtained from the dataset of Fristoe et al (2015)[8], with substitutions of congeneric species from the dataset of Wang et al (2012)[1]. Where C_{min} was available for two or more congeneric species, we chose the one with the mass nearest to the species in the Wang dataset. Body temperatures were obtained from the AnAge database[9] and other sources.

MicroRNA Families, *Binning*

Complements of conserved microRNA families were obtained from the most complete assembly for each species using the covariance model MirMachine[10], trained on the manually-curated database of microRNA genes, MirGeneDB2.1[11] (Supplementary Tables S1 and S2). For Scandentia, Lagamorpha and Rodentia, *mirFam* refers to the number of families common to Euarchontoglires. For Lorisiformes, Lemuriformes and Platyrrhini, it refers to the number of families shared with Catarrhini. For the original regression of organ *cMR*s on *mirFam* and organ size (Figure 3), *mirFam* was binned according to natural divisions in its distribution: 141 - 161 (Scandentia and Glires), 165 - 181 (Glires, Lemuriformes and Platyrrhini), and 194 - 208 (Catarrhini) (Supplementary Table S2).

Phylogenetic Trees

Using Mesquite © (2021) we derived ultrametric trees for 51 Euarchontoglires or 24 primates from the mammalian phylogeny of Alvarez-Carretero et al (2021)[12].

Variable Rate Phenograms

Variable rate trees and ancestral node values were inferred using BayesTraits.v4[13-14] (software available at www.evolution.rdg.ac.uk). Bayes factors for variable rate trees were computed from the difference between the median of the top 1% likelihoods and the median likelihood of the 1% of trees with the smallest non-zero sum of changes to branch length, *i.e.* those trees most similar to the reference time tree, as described in Fromm and Sorger (2023)[15]. Phenograms were generated using Phytools[16].

Statistics

Linear, logistic and partial least squares regressions[17-18] and normal mixture clustering[19] were carried out and visualized using JMP16®. All R^2 values were adjusted for the number of predictors.
Other than logistic regression, curves were fit empirically using the cubic spline method[20-21].
Phylogenetic linear regressions were carried out using the R: CAPER package[22].

REFERENCES (Star Methods)

1. Wang ZM, Zhang J, Ying Z and Heymsfield SB. Organ-tissue level model of resting energy expenditure across mammals: new insights into Kleiber's Law. 2012. *ISRN Zool*: 673050.

2. Navarette A, van Schaik CP and Isler K. 2011. Energetics and the evolution of human brain size. *Nature* **480**: 91-93.

3. Elia M. 1992. Organ and tissue contribution to metabolic rate. In *Energy Metabolism: Tissue Determinants and Cellular Corollaries*. Kinney JM and Tucker HN (editors), pp: 19-60. Raven Press, New York.

4. Gallagher D, Belmonte D, Deurenberg P, Wang Z, Krasnow N, Pi-Sunyer FX and Heymsfield SB. 1998. Organ-tissue mass measurement allows modeling of REE and metabolically active tissue mass. *Am J Physiol* **275**: E249–E258.

5. Grabowski M, Kopperud BT, Tsuboi M and Hansen TF. 2023. Both diet and sociality affect primate brain-size evolution. *Syst Biol* **72**: 404-418.

6. Smaers JB, Rothman RS, Hudson DR . . (many others) . . Safi K. 2021. The evolution of mammalian brain size. *Sci Adv* **7**: eabe2101.

7. Martin RD. 1993. Primate origins: plugging the gaps. *Nature* 363: 223-234.

8. Fristoe TS, Burger JR, Balk MA, Khaliq I, Hof C and Brown JH. 2015. Metabolic heat production and thermal conductance are mass-independent adaptations to thermal environment in birds and mammals. *Proc Natl Acad Sci USA* **112**: 15934-15939.

9. Magalhães JP, Abidi Z, dos Santos GA . . (many others) . . Ka Po To P. 2024. Human Ageing Genomic Resources: updates on key databases in ageing research. *Nucl Acids Res* **52**: D900-D908.

10. Umu SU, Paynter VM, Trondsøn H, Buschmann T, Rounge TB, Peterson KJ and Fromm B. 2023. Accurate microRNA annotation of animal genomes using trained covariance models of curated microRNA complements in MirMachine. *Cell Genomics* **3**: 100348.

11. Fromm B, Høye E, Domanska D, Zhong X, Aparicio-Puerta E, Ovchinnikov V, Umu SU, Chabot, PJ, Kang W, Aslanzadeh M, Tarbier M, Mármol-Sánchez E, Urgese G, Johansen M, Hovig E, Hackenberg M, Friedländer MR and Peterson KJ. 2021. MirGeneDB 2.1: toward a complete sampling of all major animal phyla. *Nucl Acids Res* **50**: D204-D210.

12. Álvarez-Carretero S, Tamuri A, Battini M, Nascimento F, Carlisle E, Asher R, Yang Z, Donoghue P and Dos Reis M. 2022. A species-level timeline of mammal evolution integrating phylogenomic data. *Nature* **602**: 263-267.

13. Pagel M, Meade A and Barker D. 2004. Bayesian estimation of ancestral character states on phylogenies. *Syst Biol* **53**: 673-684.

14. Venditti C, Meade A. and Pagel M. 2011. Multiple routes to mammalian diversity. *Nature* **479**: 393-396.

15. Fromm B and Sorger T. 2023. Rapid adaptation of cellular metabolic rate to the microRNA complements of mammals and its relevance to the evolution of endothermy. *iScience* **27**: 108740.

16. Revell LJ. 2012. phytools: an R package for phylogenetic comparative biology (and other things). *Methods Ecol Evol* **3**: 217-223.

17. de Jong S. SIMPLS: 1993. An alternative approach to partial least squares regression. *Chemometrics and Intelligent Laboratory Systems* **18**: 251-263.

18. Wold S, Johansson E. and Cocchi, M. 1993. PLS: partial least squares projections to latent structures. In *Drug Design: Theory, Methods and Applications* (pp. 523-550). Kluwer ESCOM Science Publisher.

19. Celeux G and Govaert G. Gaussian Parsimonious Clustering Models. 1995. *Pattern Recognition* **28**: 781-793.

20. Reinsch CH. 1967. Smoothing by Spline Functions. *Numerische Mathematik* 10: 177–183.

21. Eubank RL. 1999. Nonparametric regression and spline smoothing (2nd ed). CRC. Boca Raton, Florida.

22. Orme D, Freckleton RP, Thomas GH and Petzoldt T. 2013. CAPER: comparative analyses of phylogenetics and evolution in R. *Methods Ecol and Evol* **3**: 141-151.

SUPPLEMENTARY INFORMATION

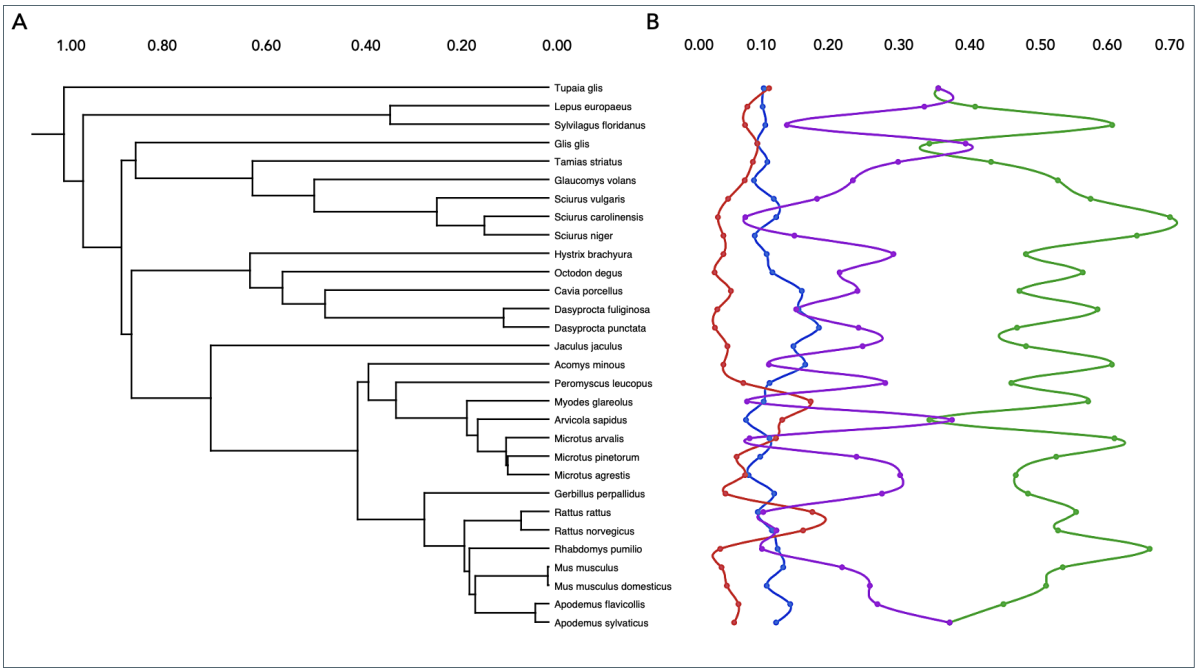

Figure S1. The proportions of brain and liver mass vary reciprocally in the Euarchontoglires Core. Species include two Lagomorpha, and 27 Rodentia, including three Sciuridae, and a Scandentia.
A. Ultrametric phylogenetic tree[12]. The scale represents the relative time of divergence.
B. Mass proportion of each organ relative to total Core mass.

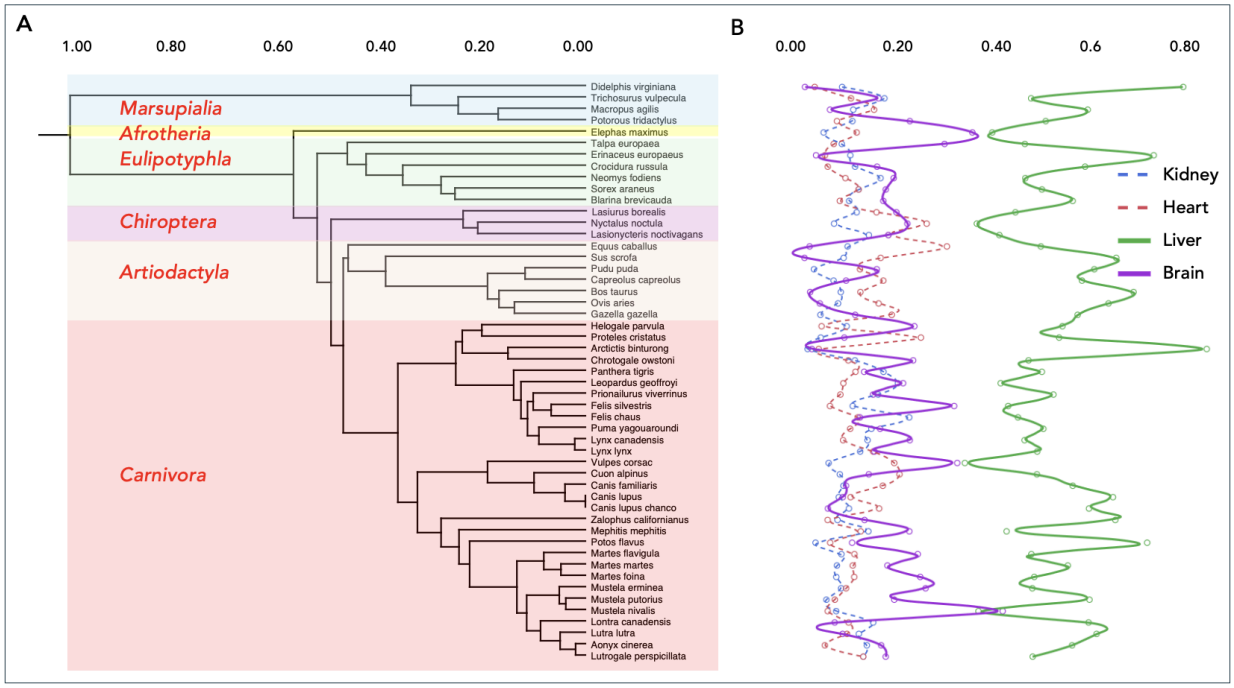

Figure S2. Core organ proportions in Metatheria, Afrotheria, and Laurasiatheria.
A. Ultrametric phylogenetic tree[12]. The scale represents the relative time of divergence.
B. Mass proportion of each organ relative to total Core mass. Note the difference in range, compared to Supplementary Figure S1-B.

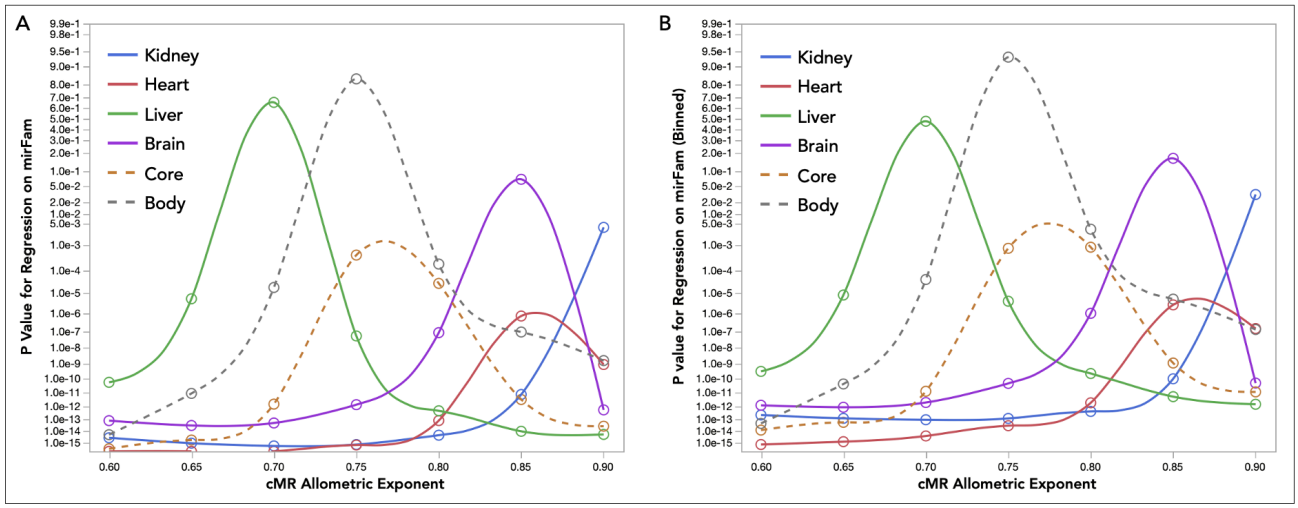

Figure S3. Dependence of *cMR* on *mirFam* or binned *mirFam* without mass correction (51 Euarchontoglires).
A. *P* values for the regression of each *cMR* on *mirFam*. Compare with Figure 3.
B. *P* values for the regression of each *cMR* on binned *mirFam*. *mirFam* was binned according to natural divisions in its distribution: 141 - 161 (Scandentia and Glires), 165 - 181 (Glires, Lemuriformes and Platyrrhini), and 194 - 208 (Catarrhini).

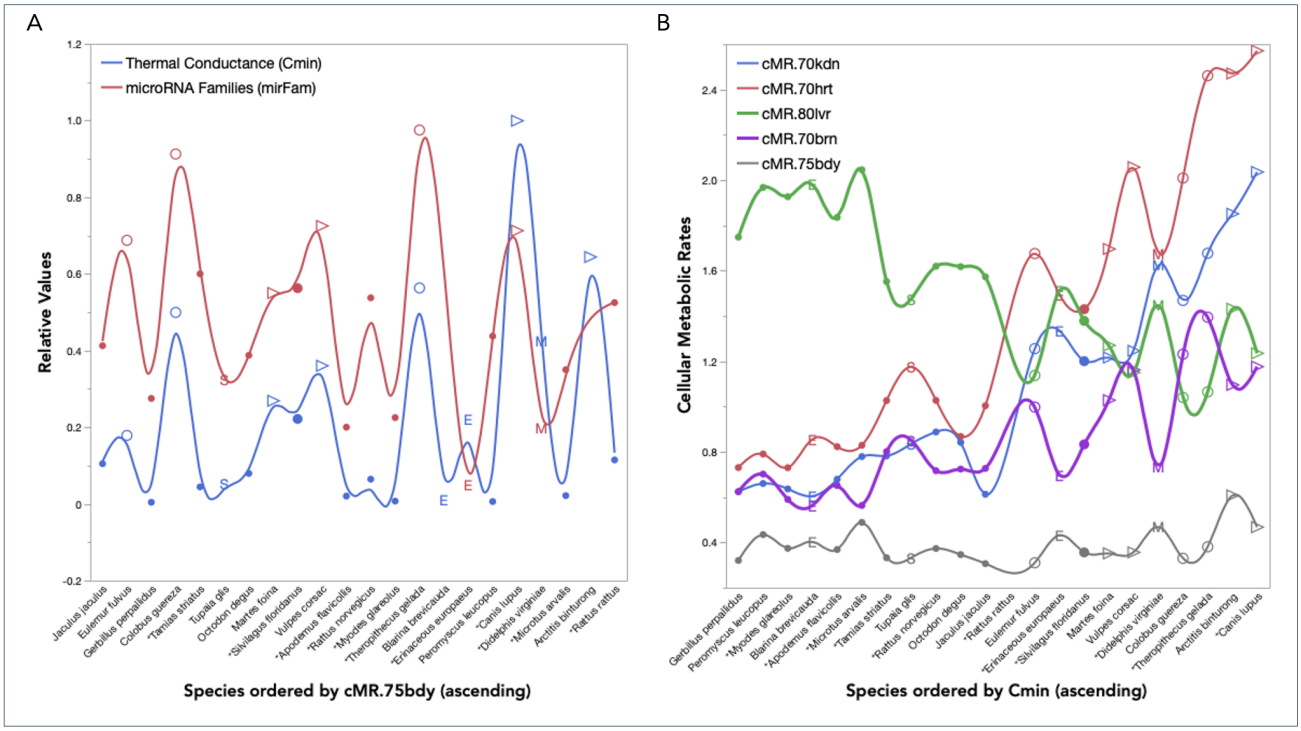

Figure S4. Core organ tradeoffs in Boreoeutheria ordered according to thermal conductance.
Legend: M - Marsupial, E - Eulypotyphla, S - Scandentia, ▷ - Carnivora, ● - Rodentia, ○ - Primata.
A. *mirFam* generally tracks C_{min} when mammals are ordered according whole body *cMR*.
B. When mammals are ordered by thermal conductance (C_{min}), the tradeoff between *cMR.70brn* and *cMR.80lvr* is apparent except among the species with the lowest values of C_{min}.
*Asterisks represent species in the 4-organ dataset of Wang et al (2012)[1] that have been substituted for congeneric species in the C_{min} dataset of Fristoe et al (2015)[8].

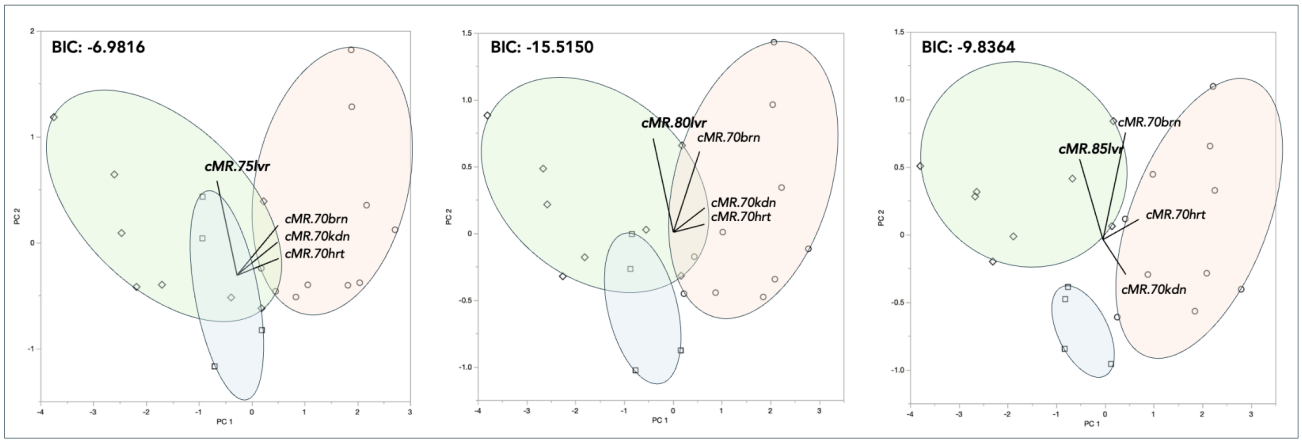

Figure S5. Unsupervised classification of primate clades based on Core *cMR* composition.
Of the four *cMR* models with *VIP* = 4 (Figure 6-B), only two (with *cMR.80lvr* and *cMR.85lvr*) resolved Platyrrhini from Lemuriformes. Principal components were calculated from each *cMR* correlation matrix, and membership in two clusters estimated by expectation maximization of their joint probability distributions (normal mixtures algorithm)[17].
BIC: Bayes Information Criterion. Liver *cMR* was varied between *cMR.75lvr* - *cMR.85lvr* (***bold type***); kidney, heart and brain *cMR* = *cMR.70*. Ellipses were hand-drawn to encompass all members of each phylogenetic clade.

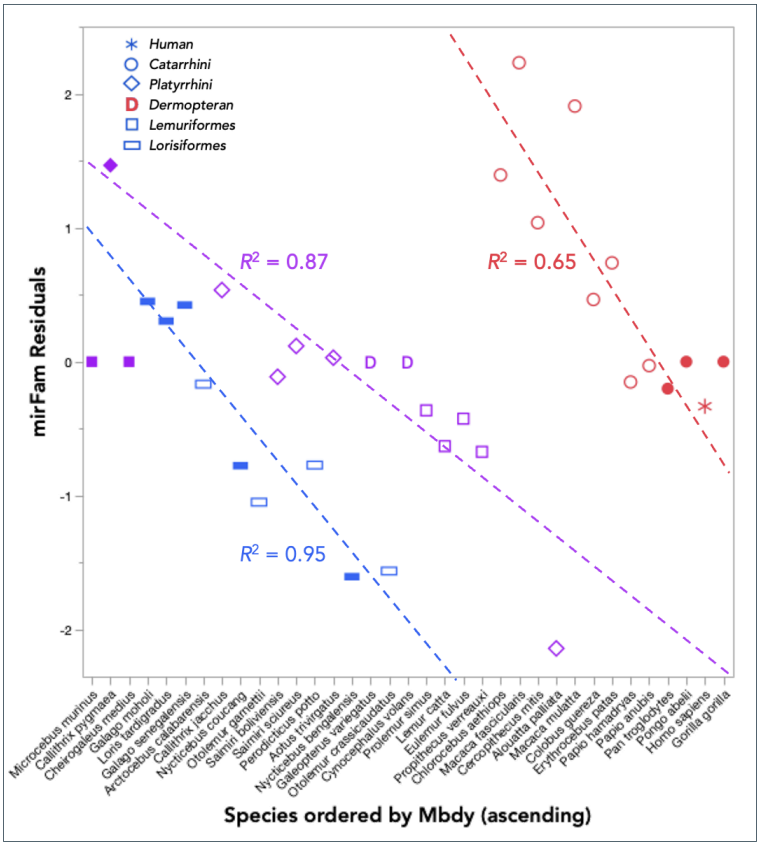

Figure S6. Conservation of *mirFam* by Clade.
The *mirFam* relationship to body size is least conserved among Catarrhini (purple). R^2 values represent the regression of residuals on Log_2*Mbdy*. For the regressions, species were grouped according to three natural divisions in the distribution of *mirFam*: Lorisiformes: 165 - 170; Lemuriformes and Platyrrhini: 171 - 180; Catarrhini: 197 - 208.
Filled symbols: circles: *Hominidae*; diamonds, rectangles: heterotherms or suspected heterotherms.

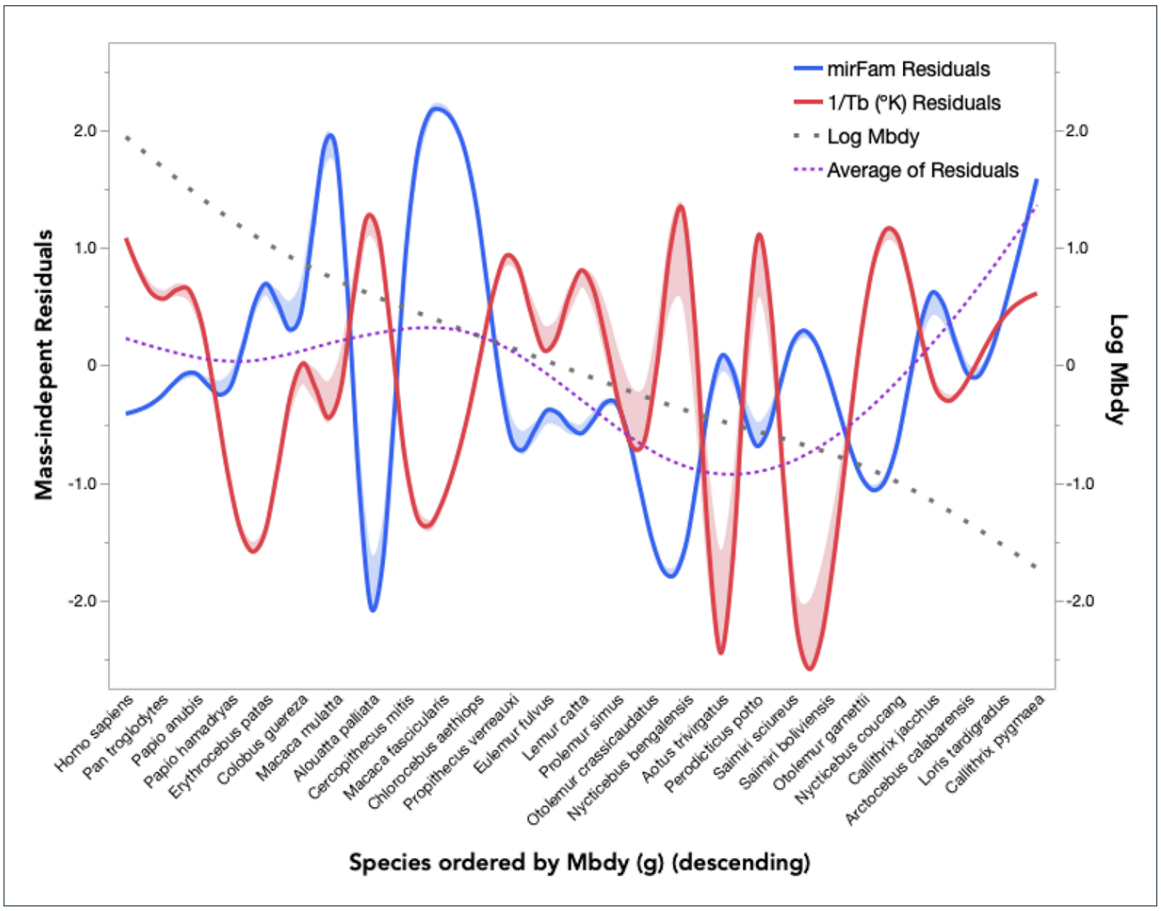

Figure S7. Reciprocal variation of *mirFam* and body temperature, $1/T_b$ (ºK).
The average of the residuals for *mirFam* and $1/T_b$ (ºK) was conserved except among the smallest primates. The values of log Mbdy and residual average were standardized. The regressions on log *Mbdy* (g) excluded six outliers (gorilla, orangutan and four small heterotherms, and two species lacked temperature data.
mirFam: R^2 = 0.70, P = 4.01e-08, N = 27. **$1/T_b$** (ºK): R^2 = 0.36, P = 9.87e-04, N = 25.
Curves were fit empirically[20-21] (cubic spline method) and shading represents confidence intervals.

Table S1. microRNA families, body mass and thermal conductance.
In order to compare organ *MR*s, species marked (*) from the dataset of Wang et al (2012)[1].
were substituted for congeneric species of similar mass in the C_{min} dataset of Fristoe et al (2015)[8].

Order	Species	*mirFam*	C_{min} (ml O_2/h/ºC)	Mass (g)	T_b (ºC)
Marsupialia	Didelphis virginiae*	141	83.97	2630	34.8
Eulipotyphla	Erinaceus europaeus*	129	45.09	950	35.2
Carnivora	Arctictis biturong		125.34	10300	36.0
Carnivora	Martes foina	169	54.08	1410	37.0
Carnivora	Canis lupus*	182	192.86	10000	36.0
Carnivora	Vulpes corsac	183	71.45	2080	
Rodentia	Apodemus flavicollis*	141	6.85	25.13	38.3
Rodentia	Myodes glareolus*	143	4.37	15.36	37.6
Rodentia	Gerbillus perpallidus	147	3.79	29.98	38.8
Rodentia	Microtus arvalis*	153	7.10	27.03	37.5
Rodentia	Microtus pinetorum*	154	4.32	21.19	37.7
Rodentia	Octodon degus	156	18.08	129.21	37.6
Rodentia	Jaculus jaculus	158	22.90	48.04	37.0
Rodentia	Peromyscus leucopus	160	4.14	22.39	36.0
Rodentia	Rattus rattus*	167	24.78	390	38.9
Rodentia	Rattus norvegicus*	168	15.24	210	37.4
Rodentia	Tamias striatus*	173	11.40	103.8	37.0
Lagomorpha	Sylvilagus floridanus*	170	83.97	972	38.3
Scandentia	Tupaia glis	151	13.36	141.1	37.0
Primata	Eulemur fulvus	180	36.91	2500	36.5
Primata	Colobus guereza	198	97.88	9750	37.0
Primata	Theropithecus gelada*	203	110	11400	37.0

Table S2. microRNA families, brain volume, body mass and temperature. Endocranial volume (ECV) and body mass were obtained from Grabowski et al (2023)[1], Smaers et al (2021)[2] (human), or estimated from Martin (1995)[3] (Dermoptera). Unless otherwise indicated, temperatures were retrieved from the AnAge database (Magalhães et al, 2024)[4].

Order	Species	*mirFam*	ECV	Mass (g)	T_b (ºC)	T_b Source
Catarrhini	Pan troglodytes	206	368.35	44967	37.2	Jensen et al (2009)[5]
Catarrhini	Homo sapiens	208	1252.00	50000	37	
Catarrhini	Gorilla gorilla	202	490.41	120950	35.5	
Catarrhini	Pongo abelii	204	65.00	3720	34.6	
Catarrhini	Chlorocebus aethiops	199	65.00	3720	36.8	
Catarrhini	Cercopithecus mitis	200	71.33	6109	37.5	
Catarrhini	Erythrocebus patas	201	97.73	9450	38	Kolka and Elizondo (1983)[6]
Catarrhini	Macaca fascicularis	207	63.98	4251	37.6	
Catarrhini	Macaca mulatta	208	88.98	6793	37.2	Von Huben et al (2007)[7]
Catarrhini	Papio hamadryas	197	146.17	14150	37.9	Brain and Mitchell (1999)[8]
Catarrhini	Papio anubis	200	167.42	18150	36.9	
Catarrhini	Colobus guereza	198	74.39	8589	37	
Platyrrhini	Callithrix pygmaea	171	4.17	116	35.2	
Platyrrhini	Callithrix jacchus	172	7.24	320	36	
Platyrrhini	Saimiri sciureus	176	24.14	799	37.5	Robinson and Fuller (1999)[9]
Platyrrhini	Saimiri boliviensis	174	25.07	789		
Platyrrhini	Aotus trivirgatus	177	16.85	989	38	
Platyrrhini	Alouatta palliata	174	49.88	6250	36	
Lemuriformes	Microcebus murinus	174	1.63	65	37.3	
Lemuriformes	Cheirogaleus medius	176	2.60	140	38	
Lemuriformes	Prolemur simus	180	27.14	2150		
Lemuriformes	Lemur catta	178	22.9	2210	36	Larsen et al (2011)[10]
Lemuriformes	Eulemur fulvus	180	25.77	2292	36.5	
Lemuriformes	Propithecus verreauxi	180	26.21	2955	36	
Lorisiformes	Galago moholi	165	3.71	148	38	Nowack et al (2023)[11]
Lorisiformes	Galago senegalensis	167	3.96	194	37.9	
Lorisiformes	Otolemur garnettii	166	11.50	764	36	
Lorisiformes	Otolemur crassicaudatus	165	11.78	1150	36.6	
Lorisiformes	Loris tardigradus	166	5.87	193	35.5	
Lorisiformes	Nycticebus coucang	167	10.13	653	35.4	
Lorisiformes	Nycticebus bengalensis	164	13.49	1060	35.5	Loris Conservation Data[12]
Lorisiformes	Arctocebus calabarensis	166	6.92	309	36.0	
Lorisiformes	Perodicticus potto	169	12.42	835	35.5	Loris Conservation Data[12]
Dermoptera	Galeopterus variegatus	177	6.9	1100		
Dermoptera	Cyanocephalus volans	173	6.9	1300		

Table S2 References

1. Grabowski M, Kopperud BT, Tsuboi M and Hansen TF. 2023. Both diet and sociality affect primate brain-size evolution. *Syst Biol* **72**: 404-418.

2. Smaers JB, Rothman RS, Hudson DR . . (many others) . . Safi K. 2021. The evolution of mammalian brain size. *Sci Adv* **7**: eabe2101.

3. Martin RD. 1993. Primate origins: plugging the gaps. *Nature* 363: 223-234.

4. Magalhães JP, Abidi Z, dos Santos GA . . (many others) . . Ka Po To P. 2024. Human Ageing Genomic Resources: updates on key databases in ageing research. *Nucl Acids Res* **52**: D900-D908.

5. Jensen SA, Mundry R, Nunn CL, Boesch C and Leendertz FH. 2009. Non-invasive body temperature measurement of wild chimpanzees using fecal temperature decline. *J Wildlife Diseases* 45: 542-546.

6. Kolka MA and Elizondo RS. 1983. Thermoregulation in Erythrocebus patas: a thermal balance study. *J Appl Physiol Respir Environ Exerc Physiol* 55: 1603-1608.

7. Von Huben SN, Lay CC, Crean RD, Davis SA, Katner SN and Taffe MA. 2007. Impact of ambient temperature on hyperthermia induced by (±)3,4-methylenedioxymethamphetamine in Rhesus Macaques. *Neuropsychopharmacol* 32: 673-681.

8. Brain C and Mitchell D. 2009. Body temperature Changes in tree-ranging baboons (*Papio hamadryas ursinus*) in the Namib Desert, Namibia. *Intl J Primatol* 4: 585-598.

9. Robinson EL and Fuller CA.1999. Endogenous thermoregulatory rhythms of squirrel monkeys in thermoneutrality and cold. *Am J Physiol* 276: *R* 1397 – *R* 1407.

10. Larsen RS, Sauther ML and Cuozzo FP. 2011. Evaluation of modified techniques for immobilization of wild ring-tailed lemurs (*Lemur catta*). *J Zoo Wildlife Med* 42: 623-633.

11. Nowack J, Mzilikazi N and Dausmann KH. 2023. Saving energy *via* short and shallow torpor bouts. *J Therm Biol* 114: 103572.

12. loris-conservation.org

Table S3. Parameters of thermodynamic Core *cMR* models for clades of Boreoeutheria and primates. For ratios of *Mbrn*/*Mbdy* and Log *Mbrn*/Log *Mbdy,* mass was expressed in mg.

Clade	N	*Mbdy* (g) (median)	med.*Mbrn* /*Mbdy*	avg.*Mbrn* /*Mbdy*	Std. Dvn.	Log *Mbrn* /Log *Mbdy*	Core cMR Exponent	Core Model R^2
Carnivora	29	5100	0.0083	0.0098	0.0048	0.6937	0.60	96.6015
Glires	26	52	0.0188	0.0190	0.0084	0.6387	0.40	99.0760
Primates	22	4300	0.0136	0.0156	0.0072	0.7080	0.53	98.0708
Platyrrhini	8	632.85	0.0235	0.0227	0.0059	0.7074	0.40	90.7004
Catarrhini	10	9125	0.0108	0.0120	0.0047	0.7182	0.60	99.3394

	Core Model Organ Coefficient				Core Model VIP Values			
Clade	***Kdn***	***Hrt***	***Lvr***	***Brn***	***Kdn***	***Hrt***	***Lvr***	***Brn***
Carnivora	0.496	0.672	0.297	0.060	1.060	1.158	0.866	0.887
Glires	0.638	0.489	0.030	-0.130	1.179	1.089	0.873	0.813
Primates	0.531	0.689	0.367	0.088	1.076	1.057	0.894	0.961
Platyrrhini	0.7111	1.1248	0.4986	-0.396	0.9414	1.1213	0.9606	0.9663
Catarrhini	0.4965	0.4058	0.2703	0.2192	`1.1111	1.1756	0.407	1.1035

Table S4. Phylogenetic regressions of organ *cMR*s on species *mirFam* (N = 22).
The dataset excluded two outliers (the human and the heterotherm *Cheirogaleus medius*).

	Allometric Exponent	Pagel's *lambda*	R^2	*P*	*AICc*
KIDNEY	0.80	0	0.5366	6.39E-05	-42.70
	0.75	0	0.5834	2.14E-05	-20.09
	0.70	0	0.5958	1.56E-05	-0.93
	0.65	0	0.5946	1.61E-05	16.22
	0.60	0	0.5859	2.00E-05	32.13
		Pagel's *lambda*	R^2	*P*	*AICc*
HEART	0.80	0	0.4937	1.60E-04	-38.02
	0.75	0	0.6476	3.83E-06	-17.88
	0.70	0	0.6962	8.44E-07	0.63
	0.65	0	0.7133	4.69E-07	17.65
	0.60	0	0.7163	4.21E-07	33.66
		Pagel's *lambda*	R^2	*P*	*AICc*
LIVER	0.80	0	0.5724	2.79E-05	-15.22
	0.75	0	0.4011	9.28E-04	-10.98
	0.70	0	0.0854	1.01E-01	-2.86
	0.65	0	-0.0344	5.89E-01	10.24
	0.60	0.962	0.0145	2.66E-01	27.34
		Pagel's *lambda*	R^2	*P*	*AICc*
BRAIN	0.80	1	0.0329	2.05E-01	-63.9
	0.75	1	0.107	7.55E-02	-35.75
	0.70	1	0.1336	5.07E-02	-10.58
	0.65	1	0.151	4.17E-02	11.76
	0.60	1	0.1596	3.71E-02	32.24